OPEN ACCESS

KING'S College LONDON

King's Research Portal

DOI:
10.1053/j.gastro.2016.05.006

Document Version
Peer reviewed version

Link to publication record in King's Research Portal

Citation for published version (APA):
Gruber, R., Panayiotou, R., Nye, E., Spencer-Dene, B., Stamp, G., & Behrens, A. (2016). YAP1 and TAZ Control Pancreatic Cancer Initiation in Mice by Direct Up-regulation of JAK-STAT3 Signaling. *Gastroenterology*, *151*(3), 526-539. https://doi.org/10.1053/j.gastro.2016.05.006

Citing this paper
Please note that where the full-text provided on King's Research Portal is the Author Accepted Manuscript or Post-Print version this may differ from the final Published version. If citing, it is advised that you check and use the publisher's definitive version for pagination, volume/issue, and date of publication details. And where the final published version is provided on the Research Portal, if citing you are again advised to check the publisher's website for any subsequent corrections.

General rights
Copyright and moral rights for the publications made accessible in the Research Portal are retained by the authors and/or other copyright owners and it is a condition of accessing publications that users recognize and abide by the legal requirements associated with these rights.

•Users may download and print one copy of any publication from the Research Portal for the purpose of private study or research.
•You may not further distribute the material or use it for any profit-making activity or commercial gain
•You may freely distribute the URL identifying the publication in the Research Portal

Take down policy
If you believe that this document breaches copyright please contact librarypure@kcl.ac.uk providing details, and we will remove access to the work immediately and investigate your claim.

Download date: 05. May. 2023

Accepted Manuscript

YAP1 and TAZ Control Pancreatic Cancer Initiation in Mice by Direct Upregulation of JAK–STAT3 Signaling

Ralph Gruber, Richard Panayiotou, Emma Nye, Bradley Spencer-Dene, Gordon Stamp, Axel Behrens

PII: S0016-5085(16)34449-3
DOI: 10.1053/j.gastro.2016.05.006
Reference: YGAST 60471

To appear in: *Gastroenterology*
Accepted Date: 14 May 2016

Please cite this article as: Gruber R, Panayiotou R, Nye E, Spencer-Dene B, Stamp G, Behrens A, YAP1 and TAZ Control Pancreatic Cancer Initiation in Mice by Direct Upregulation of JAK–STAT3 Signaling, *Gastroenterology* (2016), doi: 10.1053/j.gastro.2016.05.006.

This is a PDF file of an unedited manuscript that has been accepted for publication. As a service to our customers we are providing this early version of the manuscript. The manuscript will undergo copyediting, typesetting, and review of the resulting proof before it is published in its final form. Please note that during the production process errors may be discovered which could affect the content, and all legal disclaimers that apply to the journal pertain.

All studies published in Gastroenterology are embargoed until 3PM ET of the day they are published as corrected proofs on-line. Studies cannot be publicized as accepted manuscripts or uncorrected proofs.

ACCEPTED MANUSCRIPT

YAP1 and TAZ Control Pancreatic Cancer Initiation in Mice by Direct Upregulation of JAK–STAT3 Signaling

Ralph Gruber[1], Richard Panayiotou[2], Emma Nye[3], Bradley Spencer-Dene[3], Gordon Stamp[3], and Axel Behrens[1,4]

[1]Mammalian Genetics Laboratory
[2]Transcription Laboratory
[3]Experimental Histopathology
The Francis Crick Institute
Lincoln's Inn Fields Laboratory
44 Lincoln's Inn Fields
London WC2A 3LY, UK

[4]School of Medicine
King's College London
Guy's Campus
London SE1 1UL, UK

[*]**Corresponding author:** Dr Axel Behrens, The Francis Crick Institute, Lincoln's Inn Fields Laboratory, 44 Lincoln's Inn Fields, London WC2A 3LY, UK.
Phone: +44 207 269 3361
Fax: +44 207 269 3581
Email: Axel.Behrens@crick.ac.uk

Running title: Regulation of acinar-to-duct reprogramming by KRas

Conflict of Interest: The authors declare that they have no conflicts of interest.

Author contributions: RG conceived and designed the study, performed experiments, analyzed data, and wrote the manuscript; RP assisted with in vitro ADM assay; EN and BSD performed immunohistochemistry; GS provided histopathology analysis; AB supervised the study and wrote the manuscript.

Funding sources: This work was supported by the Francis Crick Institute, which receives its core funding from Cancer Research UK, the UK Medical Research Council, and the Wellcome Trust. R.G. was funded by an EMBO Long-Term Fellowship and a Cancer Research UK postdoctoral fellowship.

Abbreviations used in this paper: ADM, acinar-to-duct metaplasia; ChIP, chromatin immunoprecipitation; DAPI, 4',6-Diamidino-2-Phenylindole Dihydrochloride; ES, embryonic stem cell; FBS, fetal bovine serum; HBSS, Hank's balanced salt solution; IL-6, interleukin 6; mPanIN, mouse pancreatic intraepithelia neoplasia; PanIN, pancreatic intraepithelia neoplasia; PDAC, pancreatic ductal adenocarcinoma; pfu, plaque forming units; TGFα; transforming growth factor alpha; TSS, transcription start site.

ACCEPTED MANUSCRIPT

Abstract:

Background & Aims: Pancreatitis is the most important risk factor for pancreatic ductal adenocarcinoma (PDAC). Pancreatitis predisposes to PDAC because it induces a process of acinar cell reprogramming known as acinar-to-duct metaplasia (ADM)—a precursor of pancreatic intra-epithelial neoplasia lesions that can progress to PDAC. Mutations in KRAS are found at the earliest stages of pancreatic tumorigenesis, and it appears to be a gatekeeper to cancer progression. We investigated how mutations in KRAS cooperate with pancreatitis to promote pancreatic cancer progression in mice.

Methods: We generated mice carrying conditional alleles of *Yap1* and *Taz* and disrupted *Yap1* and *Taz* using a Cre-lox recombination strategy in adult mouse pancreatic acinar cells (Yap1fl/fl;Tazfl/fl;Ela1-CreERT2). We crossed these mice with LSL-KrasG12D mice, which express a constitutively active form of KRAS after Cre recombination. Pancreatic tumor initiation and progression were analyzed after chemically induced pancreatitis. We analyzed pancreatic tissues from patients with pancreatitis or PDAC by immunohistochemistry.

Results: Oncogenic activation of KRAS in normal, untransformed acinar cells in the pancreatic tissues of mice resulted in increased levels of pancreatitis-induced ADM. Expression of the constitutive active form of KRAS in this system led to activation of the transcriptional regulators YAP1 and TAZ; their function was required for pancreatitis-induced ADM in mice. The JAK–STAT3 pathway was a downstream effector of KRAS signaling via YAP1 and TAZ. YAP1 and TAZ directly mediated transcriptional activation of several genes in the JAK–STAT3 signaling pathway; this

could be a mechanism by which acinar cells that express activated KRAS become susceptible to inflammation.

Conclusion: We identified a mechanism by which oncogenic KRAS facilitates ADM and thereby generates the cells that initiate neoplastic progression. This process involves activation of YAP1 and TAZ in acinar cells, which upregulate JAK–STAT3 signaling to promote development of PDAC in mice.

KEY WORDS: PanINs, pancreatic cancer progression, mouse model, inflammation

ACCEPTED MANUSCRIPT

Introduction

The most common and lethal tumor of the pancreas, pancreatic ductal adenocarcinoma (PDAC), exhibits the histological morphology and marker expression of pancreatic duct cells. However, many of these tumors originate from the other major exocrine cell type, acinar cells, through a reprogramming process known as acinar-to-ductal metaplasia (ADM)[1]. ADM is characterized by a change in marker expression: acinar cells positive for amylase also begin to express the ductal cell marker CK19. These poorly-differentiated cells express the pancreatic progenitor cell markers Pdx1 and Nestin[2, 3] and are important precursors of malignancy[4]. Pancreatic intraepithelial neoplasia (PanIN) lesions have a well-established histological progression towards PDAC[5], and can arise from ADM lesions[1]. Thus ADM is the earliest pre-neoplastic lesion that predisposes to PDAC, making acinar-to-duct reprogramming a crucial step in pancreatic cancer initiation.

KRas mutations are found in more than 90% of all PDAC cases[6] and they occur early, in low-grade pre-neoplastic lesions[7, 8]. Although the importance of *KRas* mutation in the development of ADM, PanIN and pancreatic tumors is well established[9], the mechanisms by which oncogenic Ras leads to PDAC are not fully understood.

Pancreatitis is a well-known risk factor for PDAC development in humans. Patients with hereditary pancreatitis show a 50-fold increase in pancreatic cancer incidence[10]. In mouse models, both acute and chronic inflammation of the pancreas accelerate pancreatic cancer progression[1, 11]. Pancreatitis can be induced experimentally by injection of caerulein, which induces acinar cell death and inflammation[12]. In caerulein-induced pancreatitis, inflammation induces acinar cells to reprogram to form ADM lesions[11], which may be transient, or in the presence of a $KRas^{G12D}$ mutation, persistent[13]. TGFα administration or overexpression also cooperates with

KRas^{G12D} to induce ADM *in vitro*[3, 14]. Thus, pancreatic inflammation facilitates tumorigenesis by inducing ADM.

Expression of oncogenic *KRas*^{G12D} at endogenous levels in acinar cells triggers progression to pancreatic adenocarcinoma very inefficiently. Stronger transgenic expression of oncogenic Ras[15], or additional oncogenic stimuli, such as mutant p53[16] or TGFα overexpression[17] are required. Many of these additional stimuli directly or indirectly increase Ras activity, suggesting that a positive feedback loop amplifying oncogenic Ras signaling is required for PDAC progression[18].

The reliance of established PDAC tumors on *KRas*^{G12D} expression can be alleviated by upregulation of the transcriptional regulator YAP1[19]. YAP1 has also been implicated in progression from PanIN to PDAC[20], but its contribution at the reprogramming stage is unclear.

Here we show that *KRas* mutation sensitizes acinar cells to reprogramming by activating YAP1 and TAZ signaling, which in turn upregulates components of the JAK-STAT3 pathway. This increases sensitivity to inflammatory stimuli, which induces widespread ADM among *KRas*-mutant acinar cells. Importantly, inhibiting *KRas*^{G12D}- and pancreatitis-induced reprogramming by inactivating YAP1/TAZ also prevents progression to PanIN, underlining the importance of this mechanism for pancreatic cancer initiation.

ACCEPTED MANUSCRIPT

Materials and Methods

Mouse Lines

For the generation of conditional *Yap1* and *Taz/Wwtr1* knock-out mice, ES cell clones carrying the respective targeted alleles were obtained from the Knockout Mouse Project (KOMP) Repository (Yap1<tm1a(KOMP)Mbp>; ES clone E08) and the European Conditional Mouse Mutagenesis (EUCOMM) Program (Wwtr1<tm1a(EUCOMM)Wtsi>; ES clone A08). Targeted ES cell clones (agouti C57BL/6 parental cell line JM8A3.N1) were injected into blastocysts of C57BL/6 background to generate chimeric mice, which were then crossed with *Flpo*-expressing mice (Tg(CAG-Flpo)1Afst; C57BL/6 background)[21] to remove the neo-selection cassette and obtain mice carrying the conditional floxed alleles Yap1<tm1c(KOMP)Mbp> and Wwtr1<tm1c(EUCOMM)Wtsi> isogenic on C57BL/6. The *Flpo*-allele was bred out and mice were maintained on a C57BL/6 background. For genotyping and validation of knockout alleles, see **Supplementary Figure 4** and **Supplementary Materials and Methods**.

The *Stat3*$^{fl/fl}$, *Pdx1-Cre*, *R26-LSL-YFP*, *LSL-KRas*^{G12D} and *Ela1-Cre*^{ERT2} mouse lines have been described (see **Supplementary Materials and Methods**).

Acute pancreatitis induction

Acute pancreatitis in C57BL/6 mice was induced by eight intra-peritoneal injections of caerulein (Sigma-Aldrich) dissolved in PBS given at one-hour intervals on two consecutive days at a dose of 50 µg/kg body weight per injection (high dose). Other strains received a similar treatment schedule except with six injections at a dose of 40 µg/kg body weight per injection (low dose). Control animals received injections of PBS only.

Gene set enrichment analysis

Gene set enrichment analysis was performed on the published transcription profile of C57BL/6 Jackson mice treated with caerulein or PBS[22] and on the transcription profile of mouse liver organoids overexpressing YAP1[23], with the software developed by the Broad Institute of MIT and Harvard. The settings are listed in **Supplementary Materials and Methods**.

Primary acinar cell culture

Mice were sacrificed by cervical dislocation, the pancreas was dissected out and transferred to ice-cold Hank's balanced salt solution (HBSS) supplemented with Penicillin/Streptomycin (Sigma-Aldrich). Pancreata were cut into small pieces and digested with 2 mg/ml Collagenase P (Roche Diagnostics) in HBSS for 15 min at 37 ºC. Cells were washed three times with HBSS supplemented with 5 % FBS and then filtered through 500 μm and 105 μm nylon meshes (Spectrum Laboratories). The cell suspension was layered on top of 30 % FBS in HBSS, centrifuged at 1000 r.p.m for 2 min and the cell pellet was resuspended in acinar cell culture medium (Waymouth's medium (Life Technologies) supplemented with 1 % FBS, Penicillin/Streptomycin (Sigma-Aldrich), 1 μg/ml Dexamethasone (Sigma-Aldrich) and 100 μg/ml Soybean trypsin inhibitor (Sigma-Aldrich)). The cell suspension was then infected with adenoviruses either obtained from the University of Iowa Carver College of Medicine (Ad5-GFP and Ad5-Cre-GFP), at a concentration of $1.25x10^7$ plaque forming units (pfu)/ml, or generated by cloning (Ad-GFP, Ad-GFP-YAP1-5SA and Ad-GFP-TAZ-S89A), at a concentration of $5x10^5$ pfu/ml. Acinar cells were incubated with adenoviruses for 1 h at 37 ºC. 6-well tissue culture plates were coated with an 800 μl

layer of collagen solution (4 mg/ml rat tail collagen (BD Biosciences), 10 % 10x Waymouth's medium (Sigma-Aldrich) and 0.02 mol/l NaOH (Sigma-Aldrich)). The cell suspension was mixed 1:1 with collagen solution and plated onto the collagen layer. The acinar cell/collagen mix was allowed to solidify for 1 h at 37 ºC before adding medium. Medium was changed on day 1 and day 3 after the isolation. Quantifications were done on day 5 after isolation. To harvest the cells, the collagen matrix was digested with 1 mg/ml collagenase P (Roche Diagnostics) diluted in HBSS for 30 min at 37 ºC.

Production of recombinant adenoviruses

The vectors harboring the coding sequences of the phosphorylation mutants of YAP1 (5SA) and TAZ (S89A), kindly provided by S. Piccolo, were used to subclone the YAP1 and TAZ cDNAs in the pAd-Track-CMV vector (Addgene #16405). This results in the expression of YAP1/TAZ under the control of the CMV promoter and pAd-Track-CMV empty vector was used as control. The pAd-Track-CMV contains a GFP cDNA under control of a second CMV promoter. Recombinant adenoviruses expressing GFP, YAP1-5SA in combination with GFP or TAZ-S89A in combination with GFP were generated following the protocol as described[24]. Briefly, human HEK293A cells were co-transfected with pAd-Easy-1 (Addgene #16400) together with pAd-Track-CMV, pAd-Track-CMV-YAP1-5SA or pAd-Track-CMV-TAZ-S89A. Adenoviruses were harvested 14 days after transfection. To generate higher viral titer, fresh HEK293A were infected with the adenoviruses and grown for 7 days before harvesting and this process was repeated three times. Adenoviruses were purified using the Adeno-X Maxi Purification Kit (TaKaRa Clontech) according to the manufacturer's protocol. Virus titers were determined by infecting HEK293T cells

with a dilution series of the adenoviruses. After infection, cells were overlaid with agarose and plaques were visualized by MTT (Sigma-Aldrich) and quantified 7 days later. This protocol generated virus titer ranging from 1 to $6x10^8$ pfu/ml.

Immunoblot Analysis and Ras-GTP pulldown assay

Protein lysates were obtained from dissected pancreata, primary acinar cells or PANC1 cells and homogenized in Cell Lysis Buffer (Cell Signaling) containing proteasome inhibitor (Sigma-Aldrich). Immunoblots were performed as described[25]. PVDF membranes (GE Healthcare) were incubated with antibodies against YAP1 (Cell Signaling; #4912 and Santa Cruz; sc-15407), p-YAP1 (Ser127 in humans and Ser112 in mice; Cell Signaling; #4911); TAZ (Sigma-Aldrich; HPA007415), CK19 (DHSB; TROMA-III), STAT3 (Cell Signaling; #4904), p-STAT3 (Tyr705; Cell Signaling; #9131); LATS1 (Cell Signaling; #3477), p-LATS1 (Ser909; Cell Signaling; #9157), LIFR (Santa Cruz; sc-659), PDX1 (R&D Systems, MAB2419), SOX9 (Millipore, AB5535), p-Erk1/2 (Thr202/Tyr204; Cell Signaling; #9106), Erk1/2 (Cell Signaling, #9102), GAPDH (Abcam; ab9485) and ACTIN (Abcam; ab49900). Active Ras levels were determined by Ras-GTP pulldown assay (ThermoFisher Scientific) using the Raf Ras-binding-domain fused to GST (Raf-RBD-GST) according to the manufacturer's instructions. Signal intensities of bands were quantified using ImageJ software.

Statistics

Statistical analysis was performed using GraphPad Prism 6.0a software and 2-tailed Student's *t*-tests were used to generate *P* values. Normalized enrichment scores and nominal *P* values for the gene set enrichment analysis were generated using the

software developed by the Broad Institute of MIT and Harvard. *P* values less than 0.05 were considered significant.

Study Approval

Mouse experiments were carried out with the approval of the London Research Institute's Ethical Review Committee according to the UK Animals (Scientific Procedures) Act 1986.

ACCEPTED MANUSCRIPT

Results

YAP1 and TAZ are upregulated in pancreatitis

ADM caused by pancreatitis is an initiating step in pancreatic tumor development[1]. To find molecular regulators of this process, we performed gene set enrichment analysis[26] on the published transcriptional profile of mouse pancreata treated with caerulein[22] to identify pathways upregulated in pancreatitis (**Supplementary Figure 1A**). Many of these pathways, such as Wnt, Notch and JAK-STAT3, have previously been implicated in either acinar cell regeneration or in inducing ADM upon injury[13, 27-29]. Intriguingly, the highest gene set enrichment scores were for YAP1 target genes (**Figure 1A and Supplementary Figure 1A**).

To investigate a possible role for YAP1/TAZ signaling in pancreatitis-induced ADM, we treated C57BL/6 mice with caerulein to induce pancreatitis (**Figure 1B**). In untreated mice, YAP1 and TAZ proteins showed nuclear localization in duct cells of the pancreas, with low or absent expression in acinar cells and islet cells[20, 30] (**Supplementary Figure 1B**). Consistent with the gene set enrichment analysis, the YAP1/TAZ target genes *Ctgf*, *Cyr61*, *Ankrd1* and *Amotl2* were overexpressed in caerulein-treated animals compared with control PBS-treated mice (**Figure 1C**). Caerulein treatment reduced activatory phosphorylation of the YAP1/TAZ inhibitory kinase Lats1 (**Figure 1D and Supplementary Figure 2A and B**). In line with this, we observed increased YAP1 and TAZ protein levels (**Figure 1D and Supplementary Figure 2A and B**), accompanied by strong nuclear localization, indicating more active YAP1/TAZ in caerulein-treated animals (**Figure 1E**). Levels of the duct cell marker CK19 were also increased, consistent with acinar-to-duct reprogramming (**Figure 1D and Supplementary Figure 2A and B**). To determine the identity of the YAP1/TAZ-responsive cells we performed immunofluorescence

co-staining with pancreatic cell type specific markers. Cells co-expressing CK19 and the acinar cell marker amylase showed high levels of nuclear YAP1 and TAZ, with some stromal cells also positive (**Figure 1F**). Thus, YAP1/TAZ activity is elevated in the injured, inflamed pancreas, particularly in the subset of cells undergoing ADM.

YAP and TAZ are upregulated in ADM lesions induced by *KRas^{G12D}*

We next asked whether YAP1/TAZ upregulation is restricted to caerulein-induced ADM, or also occurs during ADM induced by oncogenic Ras. The pancreatic tumor mouse model *LSL-KRas^{G12D};Pdx1-Cre* develops PDAC with long latency and displays the whole spectrum of pre-neoplastic lesions[31] (**Figure 2A**). We found a strong signal for both YAP1 and TAZ in ADM lesions of these mice, and an upregulation of YAP1 and TAZ in pancreatic protein lysates (**Figure 2A and B and Supplementary Figure 3A and B**). Analysis of YAP1 and TAZ immunostaining on human pancreatic tissue microarrays showed strong upregulation of YAP1 in human ADM and PanIN pre-neoplastic lesions compared with normal acini (**Figure 2C-E**). TAZ was strongly upregulated in ADM and to a lesser extent in PanIN lesions in mouse models and human tissues (**Figure 2A and C-E**). Surprisingly, we found a significant downregulation of YAP1 and TAZ protein levels in human PDAC samples compared to ADM lesions (**Figure 2C-E**), suggesting a functional role of YAP1 and TAZ particularly during tumor initiation.

YAP1 and TAZ are necessary and sufficient for ADM induction

To determine the functional requirement for YAP1/TAZ signaling in acinar-to-duct reprogramming, we generated conditional floxed alleles of both *Yap1* and *Taz* (**Supplementary Figure 4A-F**). YAP1 and TAZ were efficiently deleted in

Yap1$^{fl/fl}$;*Taz*$^{fl/fl}$ primary acinar cells (**Supplementary Figure 5A and B**). We combined the floxed *Yap1*$^{fl/fl}$ and *Taz*$^{fl/fl}$ alleles with the Cre-inducible oncogenic *LSL-KRas*^{G12D} allele, shown to induce ADM in cultured acinar cells[14], and assayed ADM *in vitro* (**Figure 3A**). As expected, Cre-mediated activation of *KRas*^{G12D} transformed acinar cell clusters into tubular duct-like structures (**Figure 3B**). Deletion of *Yap1* significantly reduced the ability of *KRas*^{G12D} to induce ADM, but deletion of *Taz* did not. However, in double mutant *Yap1*/*Taz* acinar cells, *KRas*^{G12D} failed to induce ADM (**Figure 3B and Supplementary Figure 5C and D**).

To address the requirement for YAP1 *in vivo*, we combined *Yap1*$^{fl/fl}$ with the *Pdx1-Cre* mouse line. Caerulein-induced ADM lesions co-expressing CK19 and amylase were readily observed in *Yap1*$^{fl/fl}$*;Pdx1-Cre* mice. However, these lesions were positive for YAP1 nuclear staining (**Supplementary Figure 6A**), suggesting that ADM occurred in cells that had escaped *Yap1* deletion. Consistent with this, PCR and immunoblot analysis showed that the recombination efficiency and consequent depletion of YAP1 was incomplete in *Yap1*$^{fl/fl}$*;Pdx1-Cre* mice (**Supplementary Figure 6B and C**). As an alternative model, we used a tamoxifen-inducible Cre line under the control of the acinar-specific *Ela1* promoter (*Ela1-Cre*^{ERT2}) in combination with a GFP lineage tracer (*R26-LSL-YFP*) to allow identification of recombined cells (**Figure 3C**). In this model, GFP-positive acinar cells that had lost both *Yap1* and *Taz* were significantly impaired in caerulein-induced ADM formation (**Figure 3D**), supporting a requirement for YAP1 and TAZ in ADM formation *in vivo*. Importantly, co-deletion of *Yap1* and *Taz* did not affect acinar cell viability (**Supplementary Figure 7A**).

We next examined the effects of ectopic YAP1/TAZ activation in acinar cells by generating adenoviral vectors encoding constitutively active phosphorylation mutants

of YAP1 (Ad-GFP-YAP1-5SA) and TAZ (Ad-GFP-TAZ-S89A) (**Supplementary Figure 7B-D**). These mutants are predominantly nuclear and able to induce target gene expression[32, 33]: as expected, adenoviral delivery of YAP1-5SA as well as TAZ-S89A resulted in upregulation of their target genes *Ctgf* and *Cyr61* in primary acinar cells (**Supplementary Figure 7E**). Strikingly, acinar explants infected with either Ad-GFP-YAP1-5SA or Ad-GFP-TAZ-S89A, but not Ad-GFP, underwent conversion to a duct cell morphology (**Figure 3E and F**). These data suggest that activation of the transcriptional regulators YAP1 and TAZ in acinar cells is sufficient to induce ADM.

YAP1/TAZ activation increases expression of JAK-STAT3 pathway components

To investigate the molecular mechanisms downstream of YAP1/TAZ, we analyzed the published transcription profile of cells overexpressing YAP1[23]. Gene set enrichment analysis of BIOCARTA-annotated pathways in this dataset[34] identified the IL6-JAK-STAT3 signaling cascade as strongly regulated by YAP1 overexpression (**Supplementary Figure 8A**). Importantly, JAK-STAT3 signaling was also strongly upregulated in mice with pancreatitis (**Supplementary Figure 1A**), and STAT3 is known to be important for oncogenic *KRas*-induced pancreatic tumor development[28, 29, 35]. To validate the involvement of this pathway downstream of YAP1/TAZ, we analyzed the expression of JAK-STAT3 pathway components in the human PDAC cell line PANC1, which shows constitutively active YAP1/TAZ (**Supplementary Figure 8B and C**). The receptors *LIFR, GP130, IL13RA1* and the transcription factor *STAT3* were downregulated upon *YAP1* and *TAZ* knockdown in PANC1 cells (**Figure 4A**). Accordingly, *YAP1/TAZ* knockdown reduced STAT3 and LIFR protein levels (**Figure 4A and Supplementary Figure 8D**). Overexpression of constitutively active

YAP1-5SA or TAZ-S89A led to increased protein levels of STAT3 and LIFR in primary mouse acinar cells (**Figure 4B and Supplementary Figure 9A and B**).

We next tested whether the JAK-STAT3 pathway genes are direct transcriptional targets of the YAP1/TAZ-dependent TEAD transcription factors[36]. The promoter regions of *STAT3*, *LIFR* and *GP130* contain TEAD4 binding sites, as analyzed by genome-wide ENCODE chromatin immunoprecipitation (ChIP) experiments[37] (**Supplementary Figure 9C**). We confirmed that TEAD4 binding was significantly enriched at the promoters of *STAT3*, *LIFR* and *GP130* by ChIP (**Figure 4C**). In the *STAT3* promoter region, one TEAD consensus binding site GT-IIc[38] was found 312 bp to 306 bp upstream of the *STAT3* transcription start site (TSS) (**Figure 4D**). We used the entire *STAT3* promoter region including this site in a luciferase reporter construct transfected into the rat pancreatic acinar cell line AR42J. Overexpression of either YAP1-5SA or TAZ-S89A in this cell line significantly increased the luciferase activity using the *STAT3* promoter construct compared with empty vector control (**Figure 4D**). Mutation of the TEAD binding site abolished the YAP1- and TAZ-induced luciferase activity (**Figure 4D**). Deletion of *Stat3* did not change the expression or protein levels of YAP1 and TAZ in primary acinar cells (**Supplementary Figure 10A-C**). Our results suggest that, through TEAD, YAP1 and TAZ regulate the gene expression of the cytokine receptors *LIFR* and *GP130* and the transcription factor *STAT3*.

JAK-STAT3 pathway activation in ADM lesions

To examine whether JAK-STAT3 signaling is involved in ADM, we analyzed STAT3 activation in response to caerulein-induced pancreatitis. Caerulein treatment led to widespread active, phosphorylated STAT3 (pTyr705-STAT3) in the injured pancreas

(**Figure 4E**), in accordance with previous reports[29]. STAT3 phosphorylation and upregulation of STAT3 and LIFR proteins were also detected in caerulein-treated pancreas lysates (**Figure 4F and Supplementary Figure 10D and E**), and *Stat3*, *Lifr*, *Gp130* and *Jak1* were upregulated in injured pancreata at the transcriptional level (**Figure 4F**), in agreement with our bioinformatic analysis (**Supplementary Figure 1A**). Co-staining with CK19 and amylase revealed increased staining intensity of STAT3 and LIFR in *KRas*^{G12D}-induced ADM cells in the *Pdx1-Cre* model (**Supplementary Figure 11A and B**).

YAP1/TAZ-dependent extreme ADM sensitization by oncogenic *KRas*^{G12D}

The upregulation of the JAK/STAT pathway by YAP1/TAZ predicted an increased susceptibility of *KRas*^{G12D}-mutant acinar cells to inflammation, independently of oncogenic transformation. To test this, we challenged control (*R26-LSL-YFP;Ela1-Cre*^{ERT2}) and *R26-LSL-YFP;LSL-KRas*^{G12D}*;Ela1-Cre*^{ERT2} mice with caerulein to induce pancreatitis (**Figure 5A**). As expected, control mice treated with low doses of caerulein showed acinar cell loss, inflammation and a limited number of ADM lesions. However, *R26-LSL-YFP;LSL-KRas*^{G12D}*;Ela1-Cre*^{ERT2} mice displayed a dramatic increase in ADM lesions double-positive for amylase and CK19 after caerulein treatment, although the recruitment of inflammatory F4/80-positive macrophages was similar to caerulein-treated control mice (**Figure 5B, C and Supplementary Figure 12A**). Lineage tracing with the Cre-inducible *R26-LSL-YFP* allele confirmed the acinar cell origin of the ADM lesions (**Supplementary Figure 12B**). Thus oncogenic Ras mutations dramatically increase the susceptibility of acinar cells to undergo ADM, possibly by increasing acinar cell sensitivity to inflammatory cytokines through upregulation of *Stat3*, *Lifr* and *Gp130*.

We next tested the significance of YAP1/TAZ and STAT3 in Ras-induced ADM sensitization directly. Strikingly, co-deletion of *Yap1* and *Taz* completely blocked the enhanced formation of these pancreatitis-induced ADM lesions by $KRas^{G12D}$ (**Figure 5B and C**). Pancreata of *R26-LSL-YFP;LSL-*$KRas^{G12D}$*;*$Yap1^{fl/fl}$*;*$Taz^{fl/fl}$*;Ela1-*Cre^{ERT2} mice showed normal morphology with some signs of caerulein-induced acinar cell loss and inflammation similar to the extent observed in control mice (**Figure 5B and Supplementary Figure 12A**). Additionally, in agreement with previous results[29], loss of STAT3 significantly reduced caerulein-induced CK19-positive ductal structures in the mutant $KRas^{G12D}$ background (**Figure 5B and C**). Ras-induced ADM formation resulted in increased expression of the pancreatic progenitor marker Pdx1 and the duct marker Sox9, which was dependent on YAP1/TAZ (**Figure 5D and Supplementary Figure 13A**). These results suggest that expression of $KRas^{G12D}$ in normal, untransformed acinar cells results in extreme sensitization to pancreatitis-induced ADM, which is mediated by YAP1/TAZ and STAT3.

JAK-STAT3 pathway acts downstream of YAP1/TAZ in response to oncogenic Ras and inflammatory stimuli

We next addressed the function of YAP1/TAZ and JAK-STAT3 signaling as effectors of oncogenic Ras. $KRas^{G12D}$ was activated in adult acinar cells using tamoxifen-inducible *LSL-*$KRas^{G12D}$*;Ela1-*Cre^{ERT2} mice, and gene expression was analyzed 7 days later, when pancreas histology was unaltered and no tumor initiation had occurred. $KRas^{G12D}$ activation in normal untransformed acinar cells resulted in increased expression of the YAP1/TAZ target genes *Ctgf* and *Cyr61*, accompanied by transcriptional induction of *Stat3*, *Lifr* and *Gp130* (**Figure 6A**). Importantly, activation of STAT3 pathway genes by oncogenic $KRas^{G12D}$ in this context occurred

without caerulein treatment. After deletion of *Yap1*$^{fl/fl}$;*Taz*$^{fl/fl}$, *KRas*^{G12D} was unable to induce YAP1/TAZ target genes or *Stat3*, *Lifr* and *Gp130* expression (**Figure 6A**). *KRas*^{G12D} activation in primary acinar cells *in vitro* increased YAP1 and TAZ protein levels, STAT3 protein levels and STAT3 phosphorylation (**Figure 6B and Supplementary Figure 13B**) but deletion of *Yap1*$^{fl/fl}$;*Taz*$^{fl/fl}$ modestly reduced STAT3 protein levels and greatly impaired the *KRas*^{G12D}-induced phosphorylation of STAT3 in acinar cells *in vitro* (**Figure 6B and Supplementary Figure 13B**). In agreement with these results, caerulein treatment of tamoxifen-induced *LSL-KRas*^{G12D};*Ela1-Cre*^{ERT2} mice led to a dramatic increase in STAT3 phosphorylation at tyrosine 705 which was completely abolished in the absence of YAP1 and TAZ (**Figure 6C, Figure 5D and Supplementary Figure 13A**). YAP1 and TAZ deletion also diminished the caerulein-induced phosphorylation of STAT3 in pancreatic acinar cells wild type for *KRas* (**Supplementary Figure 14A and B).** These data indicate that, even in the absence of an inflammatory stimulus or tumorigenesis, oncogenic Ras mutation leads to YAP1/TAZ and JAK-STAT3 pathway activation, and YAP1 and TAZ act upstream of the JAK-STAT3 signaling pathway in oncogenic KRas-induced ADM.

Deletion of YAP1 and TAZ reduces inflammation-induced Ras activation

Inflammatory insults lead to hyperstimulation of oncogenic Ras activity, and interfering with the inflammatory signaling cascade interrupts this feedback activation[18]. We next tested whether YAP1/TAZ affects oncogenic Ras activity. Caerulein treatment increased Ras activity in mice expressing *KRas*^{G12D} in acinar cells (**Supplementary Figure 15A and B**) as shown previously[18]. Deletion of *Yap1* and *Taz* in the *KRas*^{G12D} background reduced Ras activation after caerulein treatment

(**Supplementary Figure 15A and B**). Overexpression of constitutively active YAP1 in primary acinar cells increased Ras activity (**Supplementary Figure 15C**). Hyperactivating oncogenic Ras by TGFα resulted in a more efficient differentiation of acinar to duct cells *in vitro*[39] (**Supplementary Figure 16A and B**). However, YAP1 and TAZ were required for $KRas^{G12D}$-induced ADM even in the presence of TGFα (**Supplementary Figure 16A and B**).

YAP1 and TAZ are required for $KRas^{G12D}$-induced PanIN formation

To determine whether the block to ADM in $Yap1^{fl/fl}$;$Taz^{fl/fl}$;$LSL\text{-}KRas^{G12D}$;$Ela1\text{-}Cre^{ERT2}$ mice affects the development of pancreatic cancer, we assessed PanIN lesions 3 months after the transient induction of pancreatitis by caerulein (**Figure 7A**). At this stage, $LSL\text{-}KRas^{G12D}$;$Ela1\text{-}Cre^{ERT2}$ mice displayed CK19/amylase double-positive ADM lesions and CK19- and AB/PAS-positive PanIN lesions (**Figure 7B-D**). *Yap1* and *Taz* co-deletion resulted in a striking decrease in ADM lesions and these mice were free of PanIN lesions, similar to control mice (**Figure 7B-D**). These results show that acinar cell-specific YAP1/TAZ signaling is essential for oncogenic $KRas^{G12D}$-induced PanIN formation in the context of pancreatitis, and that STAT3 signaling appears to be a critical downstream factor in this process.

Discussion

Acinar-to-duct reprogramming is now established as an important precursor to PanIN lesions and progression to pancreatic cancer, but the molecular mechanisms that drive this process have remained unclear. Our results confirm that *KRas*^{G12D} mutation synergizes with inflammatory insults to induce widespread and persistent ADM lesions, and we elucidate how this synergy occurs (**Figure 7E**). We find that the transcriptional regulators YAP1 and TAZ are required for *KRas*^{G12D} to promote acinar-to-duct reprogramming, both *in vitro* and *in vivo*. In the absence of YAP1 and TAZ, *KRas*^{G12D} is unable to induce PanIN lesions, suggesting that acinar-to-duct reprogramming via YAP1/TAZ is an obligate step in pancreatic cancer initiation from acinar cells.

Mechanistically, active YAP1 and TAZ interact with the transcription factor TEAD, which binds and upregulates the expression of several genes in the JAK-STAT3 pathway. This pathway controls the response to inflammatory cytokines like IL-6, which is secreted during caerulein-induced pancreatitis and also present at high levels in pancreatic tumors, promoting PanIN progression in *KRas*^{G12D} mice[35, 40]. A recent study found that the IL-6 coreceptor GP130, upregulated by YAP1/TAZ in our study, also activates YAP1 independently of STAT3[41]. Additionally, LIFR has been shown to act upstream of YAP1 signaling[42]. This would create a positive feedback loop amplifying YAP1 activity.

Our data in mouse models expressing *KRas*^{G12D} are consistent with findings in cultured cells showing that Ras signaling both stabilizes and activates YAP1[43, 44]. Recent studies have implicated YAP1 as an important driver of pancreatic cancer progression at later stages in collaboration with oncogenic Ras, and as a mechanism of escape from Ras-RAF-MEK-targeted therapies[19, 20, 45]. However, data from patient

samples has shown that the incidence of *KRas* codon 12 mutations is already over 90% even in the earliest pre-neoplastic lesions[8]. Here we show that YAP1 acts downstream of oncogenic Ras at this early reprogramming stage. There is likely redundancy between YAP1 and TAZ, since co-deletion of *Yap1* and *Taz* is more efficient in blocking $KRas^{G12D}$- induced ADM in the *in vitro* assay compared to either single mutant. YAP1 seems able to compensate for TAZ deletion but not vice versa; however, overexpression of constitutively active YAP1 or TAZ alone is sufficient to induce ADM.

We noted that inactivation of YAP1 and TAZ reduced ADM formation more efficiently than *Stat3* deletion (**Figure 5**). It has been shown that the Hippo pathway also interacts with other signaling pathways that have implications in ADM, such as Wnt and Notch pathways[23, 46]. YAP1/TAZ-dependent regulation of these pathways might also contribute to ADM formation.

The presence of the $KRas^{G12D}$ mutation in ADM cells in an inflammatory microenvironment is known to be sufficient for progression to PanIN lesions and pancreatic cancer[1]. Additionally, inflammation in the pancreas creates a feedback loop leading to hyperactivation of oncogenic $KRas^{G12D}$ (**Figure 7E**)[18]. The $KRas^{G12D}$ mutation and subsequent hyperactivation promotes pancreatic cancer at two levels: it creates a susceptible "cell of origin" by inducing acinar-to-duct reprogramming; and it also acts as the transforming driver that enables progression towards malignancy. This model explains why *KRas* mutations in pancreatic cancer are so common, and why they frequently appear very early, as a gatekeeper mutation, in pancreatic acinar cells.

Acknowledgements

H. Gerhardt kindly provided *Yap1*$^{fl/fl}$ mice and S. Piccolo kindly provided YAP1 (5SA) and TAZ (S89A) vectors. We thank C. Cremona and N. Tapon for comments on the manuscript and P. Chakravarty of the Francis Crick Institute Bioinformatics facility for help with gene set enrichment analysis.

ACCEPTED MANUSCRIPT

Figure legends

Figure 1. YAP1 and TAZ are upregulated in pancreatitis.

A. Gene set enrichment analysis of transcription data from caerulein-treated pancreata[22] identified enrichment of the conserved YAP1 signatures reported by Yimlamai[23] and Cordenonsi[47]. Normalized enrichment score (NES) and nominal (NOM) *P*-values are shown.

B. Scheme showing model of caerulein-induced acute pancreatitis in C57BL/6 mice.

C. Quantitative RT-PCR of YAP1/TAZ target genes in caerulein-treated versus PBS-treated pancreata. n = 3 mice each group; means ± SEM are shown; ***$P<.005$, Student's *t*-test.

D. Immunoblots of pancreas lysates from caerulein- and PBS-treated animals. p-Lats1, phosphorylated Lats1 (Ser909); p-Yap1, phosphorylated Yap1 (Ser112).

E. Immunohistochemical stains of YAP1 and TAZ in pancreata of caerulein- and PBS-treated mice. Scale bars = 50 μm. n = 5-7 mice analyzed.

F. Triple immunofluorescence of pancreata from caerulein- and PBS-treated animals showing the duct marker CK19, the acinar marker amylase and either YAP1 or TAZ. Arrowheads indicate ADM cells. Scale bars = 20 μm. n = 5-7 mice analyzed.

ACCEPTED MANUSCRIPT

Figure 2. YAP1 and TAZ are upregulated in ADM lesions induced by *KRas^{G12D}*.

A. Immunohistochemical analysis of YAP1 and TAZ in normal (*LSL-KRas^{G12D}*) pancreas and pancreas from 6-month-old *LSL-KRas^{G12D};Pdx1-Cre* mice. Scale bars = 50 μm. Dotted lines highlight mPanIN lesions. n = 4-5 mice analyzed.

B. Immunoblot analysis of pancreas lysates from control *LSL-KRas^{G12D}* and *LSL-KRas^{G12D};Pdx1-Cre* mice. p-Lats1, phosphorylated Lats1 (Ser909); p-Yap1, phosphorylated Yap1 (Ser112).

C. Immunohistochemical analysis of YAP1 and TAZ on human pancreatic tissue microarrays. Scale bars = 50 μm.

D and E. Quantification of immunohistochemical staining intensity, ranging from absent (0) to highest (6) for YAP1 (D) and TAZ (E) on human pancreatic tissue microarrays. n = number of tissue cores. Means ± SD are shown. ***P*<.01, ****P*<.005, Student's *t*-test.

Figure 3. YAP1 and TAZ are necessary and sufficient for ADM induction.

A. Scheme showing *in vitro* assay for *KRas^{G12D}*-induced ADM.

B. Brightfield images of pancreatic acinar cell clusters on day 5 after isolation from *LSL-KRas^{G12D}* and *LSL-KRas^{G12D};Yap1$^{fl/fl}$;Taz$^{fl/fl}$* mice. Cells were infected with adenoviruses encoding either GFP (Ad-GFP) or GFP plus Cre (Ad-Cre) on day 0. White arrows: tubular ductal structures. Scale bars = 50 μm. Quantification of tubular

ductal structures of the indicated genotypes with n = 3-4 mice per group; means ± SEM are shown; ***P<.005, n.s. = not significant, Student's *t*-test.

C. Experimental design of caerulein-induced acute pancreatitis in the acinar-specific and tamoxifen-inducible *Ela1-Cre^{ERT2}* mouse model combined with the *R26-LSL-YFP* lineage tracer.

D. Triple immunofluorescence of pancreata from *R26-LSL-YFP;Ela1-Cre^{ERT2}* and *R26-LSL-YFP;Yap1$^{fl/fl}$;Taz$^{fl/fl}$;Ela1-Cre^{ERT2}* mice treated with caerulein as indicated in C. Scale bars = 20 μm. Dotted white lines indicate ADM lesions. Quantification of GFP-positive ADM cells (CK19/Amylase double positive) as a percentage of total GFP-positive cells in caerulein-treated mice of the indicated genotypes. n = 3 mice per group; means ± SEM are shown; **P<.01, Student's *t*-test.

E. Scheme showing *in vitro* assay for YAP1 and TAZ-induced ADM.

F. Brightfield images (upper panels) and GFP signal (lower panels) of acinar cells after 5 days in culture, infected on day 0 with Ad-GFP, Ad-YAP1-5SA-GFP or Ad-TAZ-S89A-GFP. Scale bars = 25 μm. Quantification of GFP-positive tubular ductal structures at day 5, in n = 3 experiments; means ± SEM are shown; ***P<.005, Student's *t*-test.

ACCEPTED MANUSCRIPT

Figure 4. YAP1/TAZ activation controls JAK-STAT3 signaling via transcription of STAT3.

A. Quantitative RT-PCR of the indicated genes and immunoblots of lysates from PANC1 cells expressing shRNAs against YAP1 and TAZ (shYAP/TAZ-#1 and -#2) or non-targeted shRNA control (shNT). n = 3; means ± SEM shown.

B. Immunoblots of primary acinar cell lysates 2 days after isolation and infection with Ad-GFP, Ad-YAP1-5SA-GFP or Ad-TAZ-S89A-GFP.

C. Quantitative ChIP-PCR of the *LIFR*, *GP130* and *STAT3* loci (promoter and intron regions) using either IgG or an antibody against TEAD4. ZFP37 intron = negative control region; CTGF promoter = positive control region. n = 3 experiments; means ± SEM shown.

D. Scheme showing luciferase expression construct with human *STAT3* promoter region. Base pair (bp) numbers indicate position relative to *STAT3* transcription start site. Red box indicates GT-IIc TEAD binding motif; genomic sequence of WT GT-IIc shown below. Mutant *STAT3* promoter construct with a six-base-pair deletion of the GT-IIc site (mut GT-IIc) was used as control. Luciferase expression analysis using WT and mutant *STAT3* promoter regions in AR42J acinar cells one day after transfection with empty vector, YAP1-5SA or TAZ-S89A. An artificial TEAD luciferase reporter consisting of eight GT-IIc motifs was used as positive control. n = 3-5 experiments; means ± SEM shown.

E. Immunohistochemistry showing phosphorylated STAT3 (Tyr705) in pancreata of caerulein- and PBS-treated C57BL/6 mice. Scale bars = 50 μm. n = 3 mice analyzed.

F. Immunoblots of pancreas lysates from PBS- and caerulein-treated animals on day 2 and day 7 after treatment. p-Stat3, phosphorylated Stat3 (Tyr705). Quantitative RT-

PCR of JAK-STAT3 pathway genes in caerulein-treated vs. PBS-treated pancreata 2 days after treatment. n = 3-4 mice per group; means ± SEM shown. **P*<.05, ***P*<.01, ****P*<.005, n.s. = not significant, Student's *t*-test.

Figure 5. YAP1 and TAZ are required for *KRas*^{G12D}-induced ADM *in vivo* in response to pancreatitis.

A. Scheme showing experimental design of caerulein-induced acute pancreatitis in cooperation with acinar-specific *KRas*^{G12D} mutation.

B. H&E stain and amylase and CK19 antibody stains of pancreata from mice of the indicated genotypes. Scale bars: H&E (top row) 2 mm; (2nd row) 200 μm; (3rd row) 50 μm; Amylase 200 μm; CK19 (5th row) 200 μm; (6th row) 50 μm; double immunofluorescence 50 μm.

C. Quantification of CK19+amylase+ ADM pancreatic area in pancreatic sections of the genotypes shown in (B). n = 3 mice per genotype; means ± SEM are shown; ****P*<.005, Student's *t*-test.

D. Immunoblots of pancreas lysates from mice of the indicated genotypes treated as shown in (A).

ACCEPTED MANUSCRIPT

Figure 6. *KRas^{G12D}*- and caerulein-mediated activation of STAT3 depends on YAP1 and TAZ.

A. Quantitative RT-PCR of the YAP1/TAZ target genes *Ctgf*, *Cyr61* and *Amotl2* and the STAT3 pathway genes *Stat3*, *Lifr*, and *Gp130* in pancreas lysates from *Ela1-Cre^{ERT2}*, *LSL-KRas^{G12D};Ela1-Cre^{ERT2}* and *LSL-KRas^{G12D};Yap1$^{fl/fl}$;Taz$^{fl/fl}$;Ela1-Cre^{ERT2}* mice 7 days after the last tamoxifen injection. n = 3-5 mice per genotype; means ± SEM are shown; **P*<.05; ***P*<.01; n.s. = not significant, Student's *t*-test.

B. Immunoblot analysis of primary acinar cells from WT, *LSL-KRas^{G12D}* and *LSL-KRas^{G12D};Yap1$^{fl/fl}$;Taz$^{fl/fl}$* mice, 2 days after isolation and infection with Ad-Cre adenovirus. pStat3, phosphorylated Stat3 (Tyr705).

C. Immunohistochemistry with antibodies against phosphorylated STAT3 (Tyr705) and STAT3 in pancreata of the indicated genotypes. Mice were treated with tamoxifen and caerulein as indicated in Figure 5A. Scale bars = 50 μm. n = 3-5 mice analyzed.

ACCEPTED MANUSCRIPT

Figure 7. YAP1 and TAZ are required for *KRas^{G12D}*-induced PanIN.

A. Scheme showing experimental design of caerulein-induced PanIN formation in the *KRas^{G12D}* background.

B. H&E, amylase and CK19 antibody, and AB/PAS stains of pancreata from mice of the indicated genotypes. Scale bars: H&E 200 μm; CK19 200 μm; double immunofluorescence 50 μm; AB/PAS (4th row) 200 μm; AB/PAS (5th row) 50 μm.

C. Quantification of CK19+amylase+ ADM lesions in control, *LSL-KRas^{G12D};Ela1-Cre^{ERT2}* and *LSL-KRas^{G12D};Yap1$^{fl/fl}$;Taz$^{fl/fl}$;Ela1-Cre^{ERT2}* mice. n = 3-4 mice per genotype; means ± SEM are shown; **P*<.05, Student's *t*-test.

D. Quantification of AB/PAS-positive PanIN lesions in control, *LSL-KRas^{G12D};Ela1-Cre^{ERT2}* and *LSL-KRas^{G12D};Yap1$^{fl/fl}$;Taz$^{fl/fl}$;Ela1-Cre^{ERT2}* mice. n = 3-4 mice per group; means ± SEM are shown; **P*<.05, Student's *t*-test.

E. Scheme showing the roles of YAP1 and TAZ in pancreatic cancer initiation by inducing ADM in response to oncogenic *KRas^{G12D}* and inflammation. See text for details.

ACCEPTED MANUSCRIPT

References

1. Guerra C, Schuhmacher AJ, Canamero M, et al. Chronic pancreatitis is essential for induction of pancreatic ductal adenocarcinoma by K-Ras oncogenes in adult mice. Cancer Cell 2007;11:291-302.

2. Jensen JN, Cameron E, Garay MV, et al. Recapitulation of elements of embryonic development in adult mouse pancreatic regeneration. Gastroenterology 2005;128:728-41.

3. Means AL, Meszoely IM, Suzuki K, et al. Pancreatic epithelial plasticity mediated by acinar cell transdifferentiation and generation of nestin-positive intermediates. Development 2005;132:3767-76.

4. Reichert M, Rustgi AK. Pancreatic ductal cells in development, regeneration, and neoplasia. J Clin Invest 2011;121:4572-8.

5. Hruban RH, Adsay NV, Albores-Saavedra J, et al. Pancreatic intraepithelial neoplasia: a new nomenclature and classification system for pancreatic duct lesions. Am J Surg Pathol 2001;25:579-86.

6. Biankin AV, Waddell N, Kassahn KS, et al. Pancreatic cancer genomes reveal aberrations in axon guidance pathway genes. Nature 2012;491:399-405.

7. DiGiuseppe JA, Hruban RH, Offerhaus GJ, et al. Detection of K-ras mutations in mucinous pancreatic duct hyperplasia from a patient with a family history of pancreatic carcinoma. Am J Pathol 1994;144:889-95.

ACCEPTED MANUSCRIPT

8. Kanda M, Matthaei H, Wu J, et al. Presence of somatic mutations in most early-stage pancreatic intraepithelial neoplasia. Gastroenterology 2012;142:730-733 e9.

9. Eser S, Schnieke A, Schneider G, et al. Oncogenic KRAS signalling in pancreatic cancer. Br J Cancer 2014;111:817-22.

10. Bardeesy N, DePinho RA. Pancreatic cancer biology and genetics. Nat Rev Cancer 2002;2:897-909.

11. Carriere C, Young AL, Gunn JR, et al. Acute pancreatitis markedly accelerates pancreatic cancer progression in mice expressing oncogenic Kras. Biochem Biophys Res Commun 2009;382:561-5.

12. Hofbauer B, Saluja AK, Lerch MM, et al. Intra-acinar cell activation of trypsinogen during caerulein-induced pancreatitis in rats. Am J Physiol 1998;275:G352-62.

13. Morris JPt, Cano DA, Sekine S, et al. Beta-catenin blocks Kras-dependent reprogramming of acini into pancreatic cancer precursor lesions in mice. J Clin Invest 2010;120:508-20.

14. **Shi G**, **DiRenzo D**, **Qu C**, et al. Maintenance of acinar cell organization is critical to preventing Kras-induced acinar-ductal metaplasia. Oncogene 2013;32:1950-8.

15. Ji B, Tsou L, Wang H, et al. Ras activity levels control the development of pancreatic diseases. Gastroenterology 2009;137:1072-82, 1082 e1-6.

16. Hingorani SR, Wang L, Multani AS, et al. Trp53R172H and KrasG12D cooperate to promote chromosomal instability and widely metastatic pancreatic ductal adenocarcinoma in mice. Cancer Cell 2005;7:469-83.

17. Siveke JT, Einwachter H, Sipos B, et al. Concomitant pancreatic activation of Kras(G12D) and Tgfa results in cystic papillary neoplasms reminiscent of human IPMN. Cancer Cell 2007;12:266-79.

18. Daniluk J, Liu Y, Deng D, et al. An NF-kappaB pathway-mediated positive feedback loop amplifies Ras activity to pathological levels in mice. J Clin Invest 2012;122:1519-28.

19. **Kapoor A**, **Yao W**, **Ying H**, et al. Yap1 activation enables bypass of oncogenic Kras addiction in pancreatic cancer. Cell 2014;158:185-97.

20. Zhang W, Nandakumar N, Shi Y, et al. Downstream of mutant KRAS, the transcription regulator YAP is essential for neoplastic progression to pancreatic ductal adenocarcinoma. Sci Signal 2014;7:ra42.

21. Kranz A, Fu J, Duerschke K, et al. An improved Flp deleter mouse in C57Bl/6 based on Flpo recombinase. Genesis 2010;48:512-20.

22. Ulmasov B, Oshima K, Rodriguez MG, et al. Differences in the degree of cerulein-induced chronic pancreatitis in C57BL/6 mouse substrains lead to new insights in identification of potential risk factors in the development of chronic pancreatitis. Am J Pathol 2013;183:692-708.

23. **Yimlamai D**, **Christodoulou C**, Galli GG, et al. Hippo pathway activity influences liver cell fate. Cell 2014;157:1324-38.

24. He TC, Zhou S, da Costa LT, et al. A simplified system for generating recombinant adenoviruses. Proc Natl Acad Sci U S A 1998;95:2509-14.

25. Gruber R, Zhou Z, Sukchev M, et al. MCPH1 regulates the neuroprogenitor division mode by coupling the centrosomal cycle with mitotic entry through the Chk1-Cdc25 pathway. Nat Cell Biol 2011;13:1325-34.

26. **Subramanian A**, **Tamayo P**, Mootha VK, et al. Gene set enrichment analysis: a knowledge-based approach for interpreting genome-wide expression profiles. Proc Natl Acad Sci U S A 2005;102:15545-50.

27. Miyamoto Y, Maitra A, Ghosh B, et al. Notch mediates TGF alpha-induced changes in epithelial differentiation during pancreatic tumorigenesis. Cancer Cell 2003;3:565-76.

28. Corcoran RB, Contino G, Deshpande V, et al. STAT3 plays a critical role in KRAS-induced pancreatic tumorigenesis. Cancer Res 2011;71:5020-9.

29. **Fukuda A**, **Wang SC**, Morris JPt, et al. Stat3 and MMP7 contribute to pancreatic ductal adenocarcinoma initiation and progression. Cancer Cell 2011;19:441-55.

30. George NM, Day CE, Boerner BP, et al. Hippo signaling regulates pancreas development through inactivation of Yap. Mol Cell Biol 2012;32:5116-28.

31. Hingorani SR, Petricoin EF, Maitra A, et al. Preinvasive and invasive ductal pancreatic cancer and its early detection in the mouse. Cancer Cell 2003;4:437-50.

32. Zhao B, Wei X, Li W, et al. Inactivation of YAP oncoprotein by the Hippo pathway is involved in cell contact inhibition and tissue growth control. Genes Dev 2007;21:2747-61.

33. Lei QY, Zhang H, Zhao B, et al. TAZ promotes cell proliferation and epithelial-mesenchymal transition and is inhibited by the hippo pathway. Mol Cell Biol 2008;28:2426-36.

34. **Huang DW**, **Sherman BT**, Lempicki RA. Systematic and integrative analysis of large gene lists using DAVID bioinformatics resources. Nat Protoc 2009;4:44-57.

35. Lesina M, Kurkowski MU, Ludes K, et al. Stat3/Socs3 activation by IL-6 transsignaling promotes progression of pancreatic intraepithelial neoplasia and development of pancreatic cancer. Cancer Cell 2011;19:456-69.

36. Mahoney WM, Jr., Hong JH, Yaffe MB, et al. The transcriptional co-activator TAZ interacts differentially with transcriptional enhancer factor-1 (TEF-1) family members. Biochem J 2005;388:217-25.

37. ENCODE Project Consortium. An integrated encyclopedia of DNA elements in the human genome. Nature 2012;489:57-74.

38. Home P, Saha B, Ray S, et al. Altered subcellular localization of transcription factor TEAD4 regulates first mammalian cell lineage commitment. Proc Natl Acad Sci U S A 2012;109:7362-7.

39. **Eser S**, **Reiff N**, **Messer M**, et al. Selective requirement of PI3K/PDK1 signaling for Kras oncogene-driven pancreatic cell plasticity and cancer. Cancer Cell 2013;23:406-20.

40. Suzuki S, Miyasaka K, Jimi A, et al. Induction of acute pancreatitis by cerulein in human IL-6 gene transgenic mice. Pancreas 2000;21:86-92.

41. Taniguchi K, Wu LW, Grivennikov SI, et al. A gp130-Src-YAP module links inflammation to epithelial regeneration. Nature 2015;519:57-62.

42. Chen D, Sun Y, Wei Y, et al. LIFR is a breast cancer metastasis suppressor upstream of the Hippo-YAP pathway and a prognostic marker. Nat Med 2012;18:1511-7.

43. **Hong X**, **Nguyen HT**, Chen Q, et al. Opposing activities of the Ras and Hippo pathways converge on regulation of YAP protein turnover. EMBO J 2014;33:2447-57.

44. Reddy BV, Irvine KD. Regulation of Hippo signaling by EGFR-MAPK signaling through Ajuba family proteins. Dev Cell 2013;24:459-71.

45. Lin L, Sabnis AJ, Chan E, et al. The Hippo effector YAP promotes resistance to RAF- and MEK-targeted cancer therapies. Nat Genet 2015;47:250-6.

46. Azzolin L, Panciera T, Soligo S, et al. YAP/TAZ incorporation in the beta-catenin destruction complex orchestrates the Wnt response. Cell 2014;158:157-70.

ACCEPTED MANUSCRIPT

47. Cordenonsi M, Zanconato F, Azzolin L, et al. The Hippo transducer TAZ confers cancer stem cell-related traits on breast cancer cells. Cell 2011;147:759-72.

Author names in bold designate shared co-first authorship.

ACCEPTED MANUSCRIPT

Gruber Figure 1

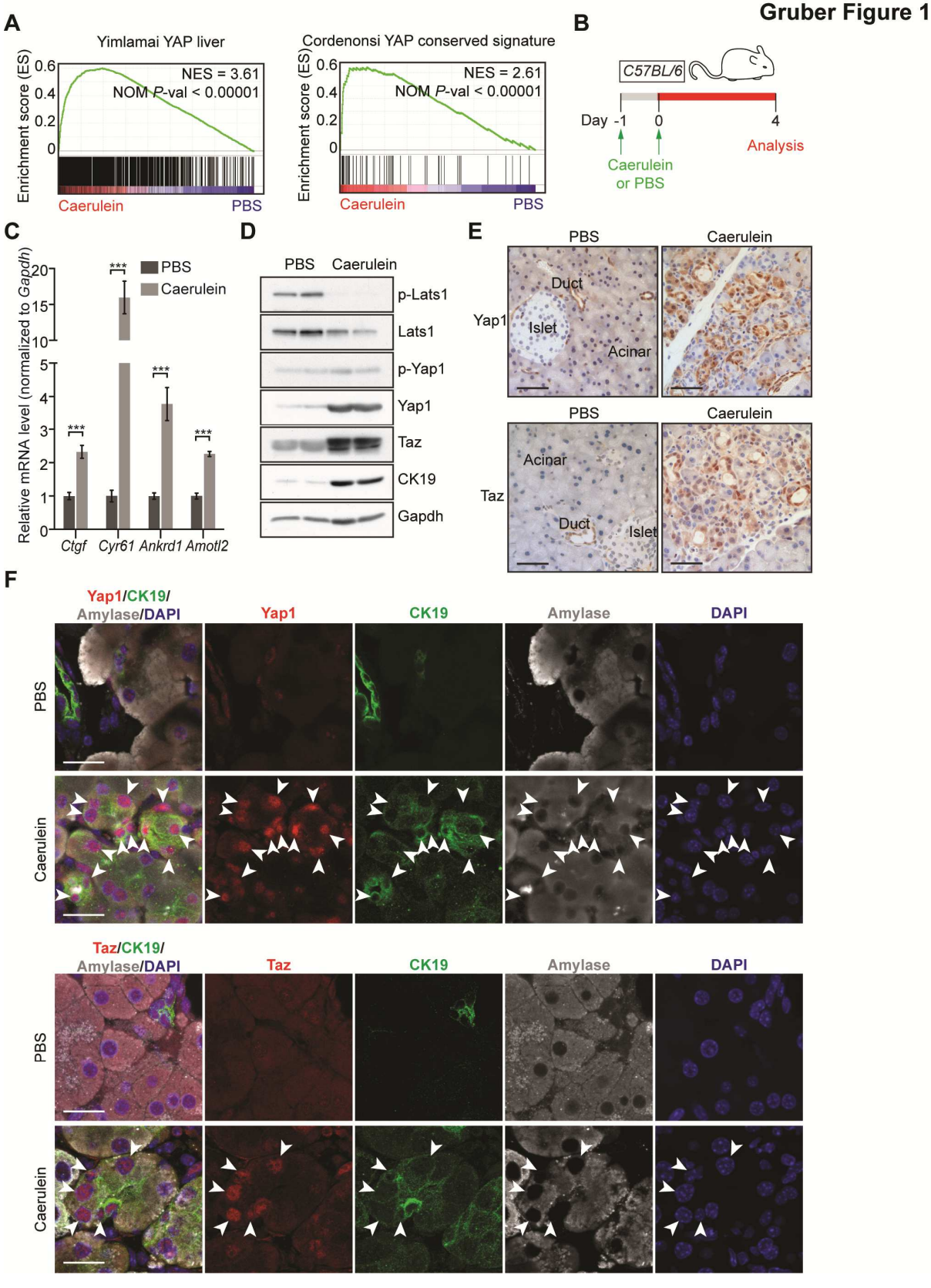

Gruber Figure 2

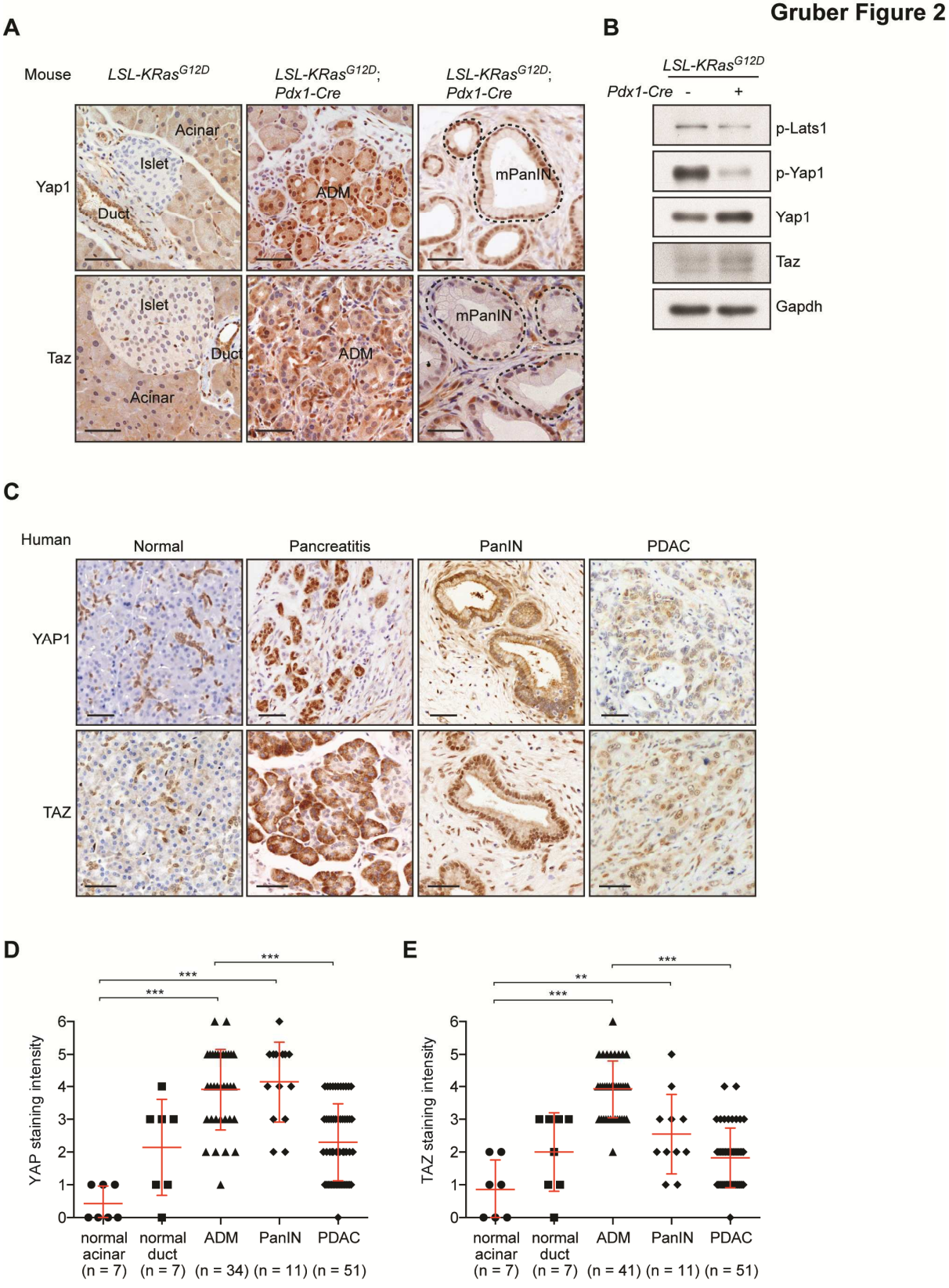

Gruber Figure 3

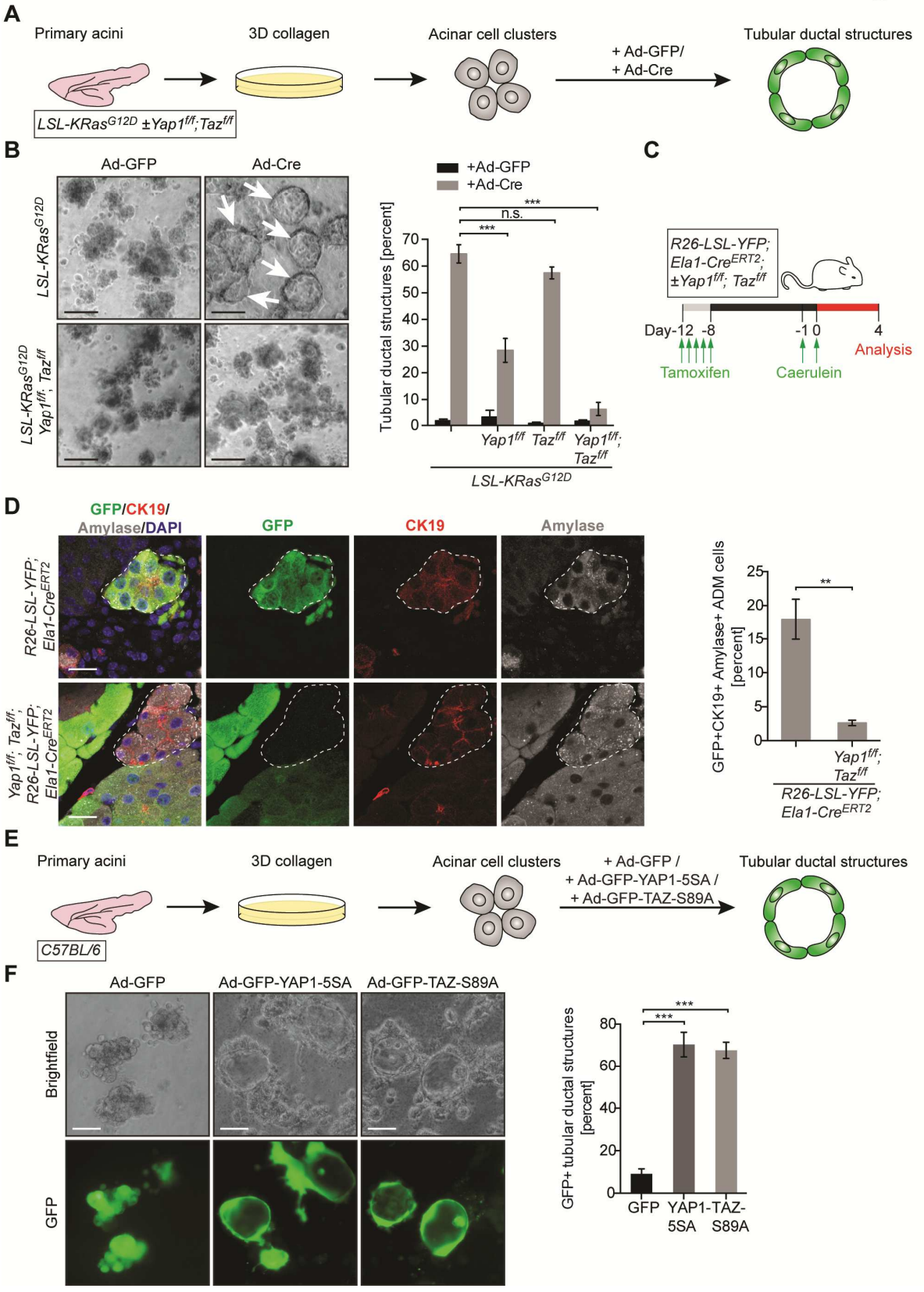

Gruber Figure 4

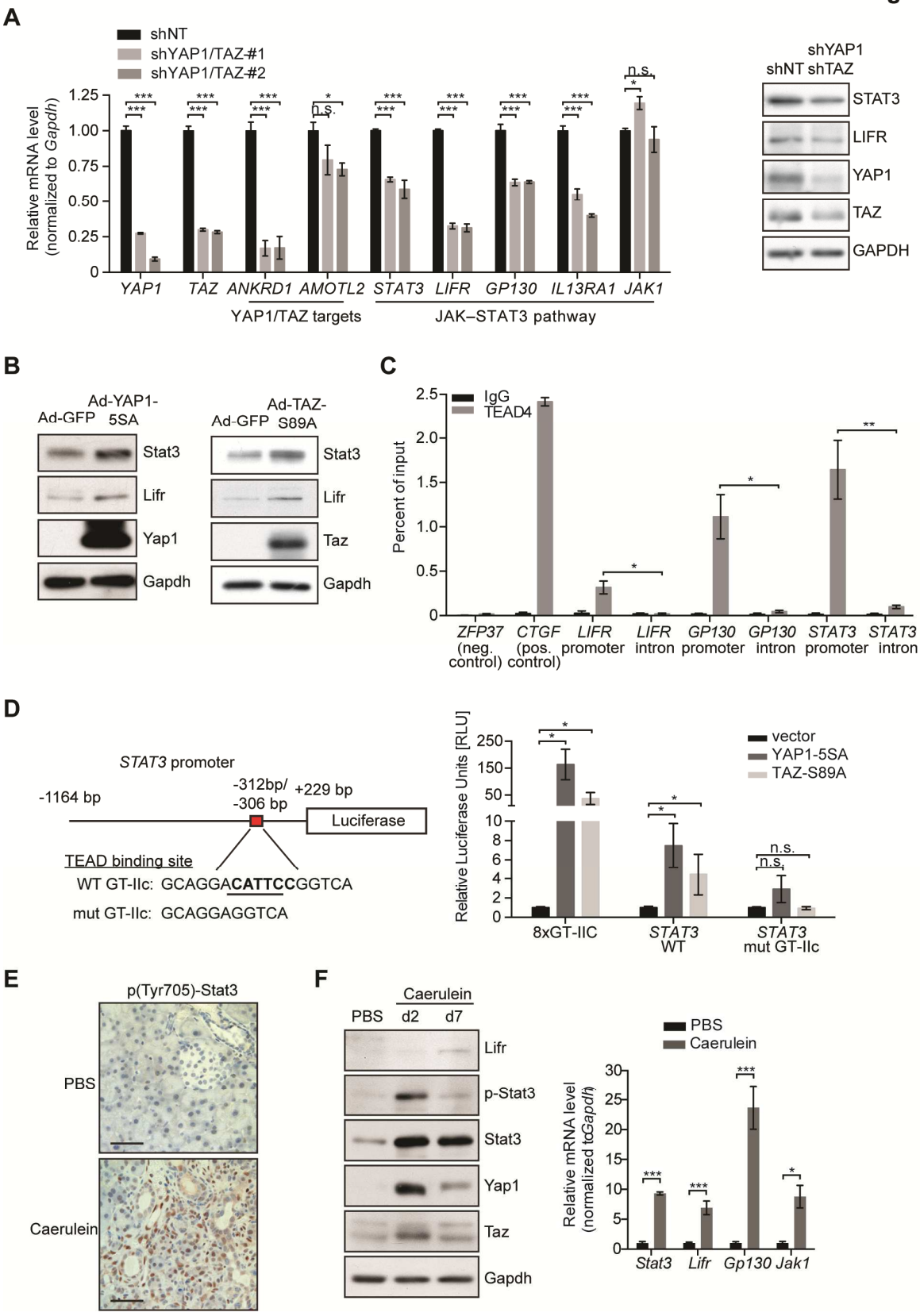

Gruber Figure 5

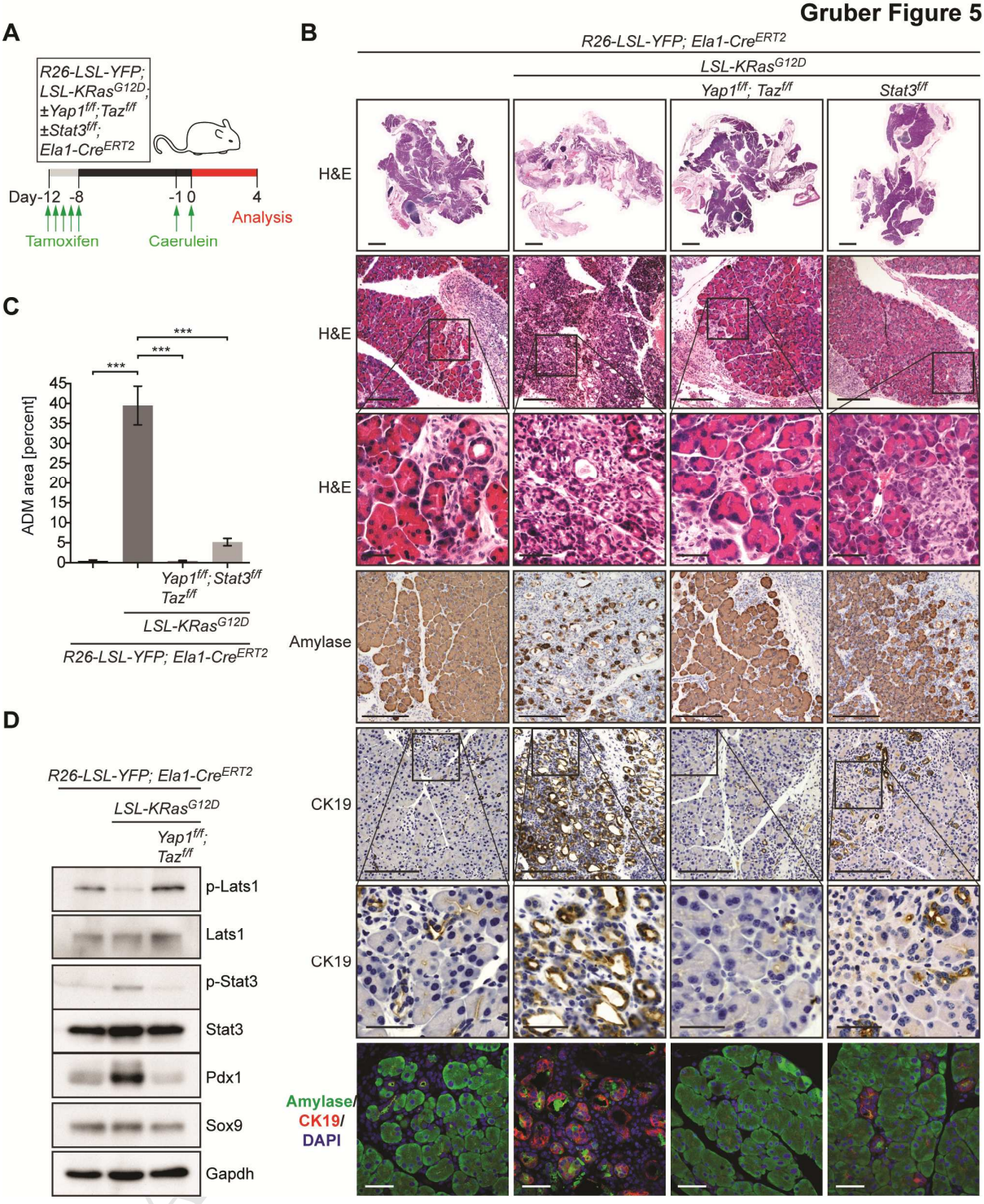

ACCEPTED MANUSCRIPT

Gruber Figure 6

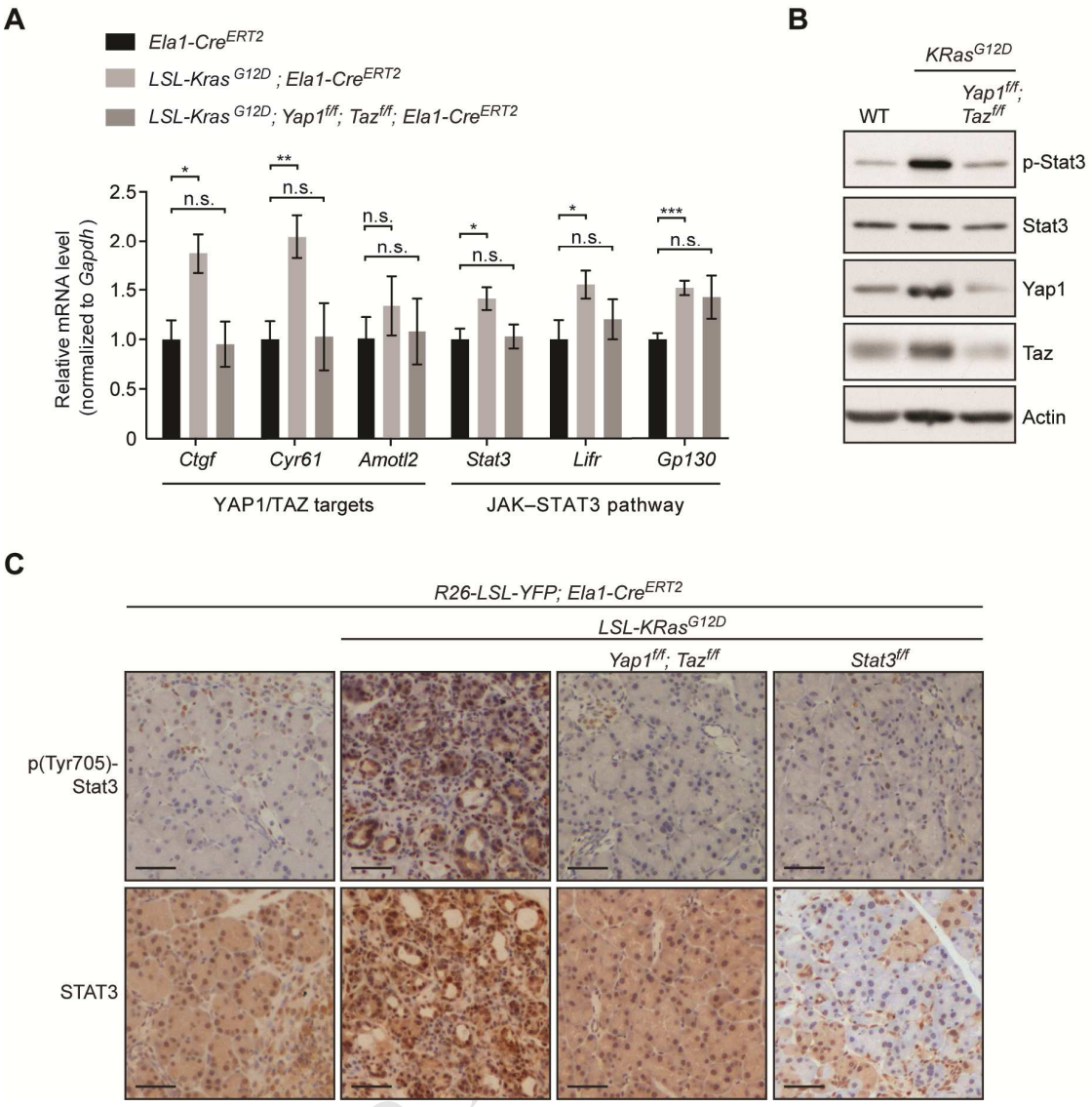

Gruber Figure 7

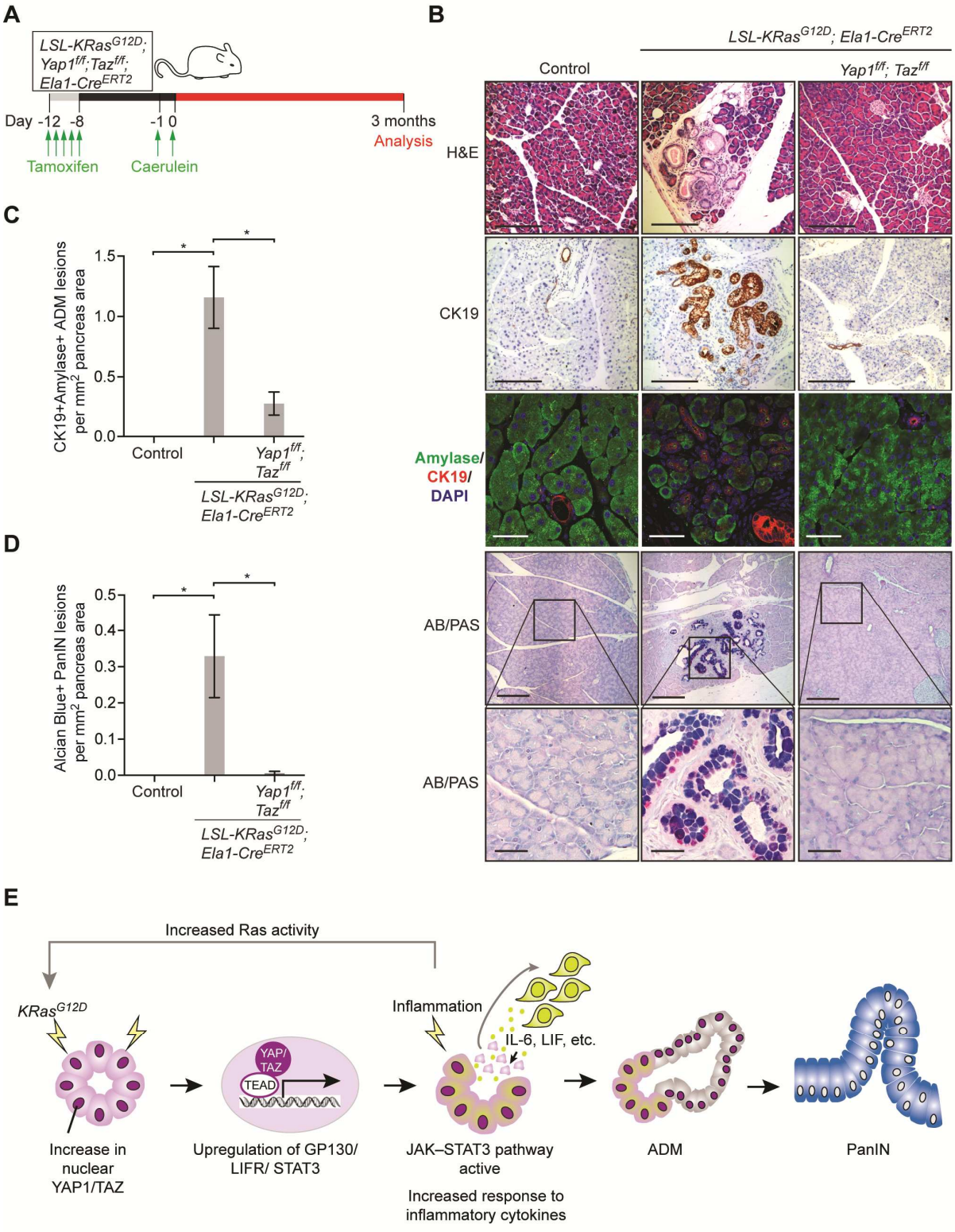

A

Gene signature	Normalized enrichment score	NOM *P*-value	Reference
YIMLAMAI_YAP_LIVER	**3.61486**	**<.00001**	7
CORDENONSI_YAP_CONSERVED_SIGNATURE	**2.77745**	**<.00001**	8
LABBE_WNT3A_TARGETS_UP	2.68678	<.00001	9
YAP_ZHAO_MCF10AND3T3	**2.61143**	**<.00001**	10
REACTOME_SIGNALING_BY_WNT	2.46385	<.00001	11, 12
DANG_MYC_TARGETS_UP	2.46289	<.00001	13
ALFANO_MYC_TARGETS	2.41509	<.00001	14
HAN_JNK_SIGNALING_UP	2.36262	<.00001	15
ABBUD_LIF_SIGNALING_1_UP	2.27401	<.00001	16
PID_IL6_PATHWAY	2.16067	<.00001	17
MTOR_UP.V1_UP	2.15835	<.00001	18
HINATA_NFKB_TARGETS_FIBROBLAST_UP	2.10119	<.00001	19
DASU_IL6_SIGNALING_UP	1.94122	<.00001	20
AZARE_STAT3_TARGETS	1.87138	=.00642	21
PARENT_MTOR_SIGNALING_UP	1.78848	<.00001	22
DAUER_STAT3_TARGETS_UP	1.73730	<.00001	23
NGUYEN_NOTCH1_TARGETS_UP	1.61923	=.02371	24
VILIMAS_NOTCH1_TARGETS_UP	1.60965	=.00873	25
TGFB_UP.V1_UP	1.39460	=.01903	26

B

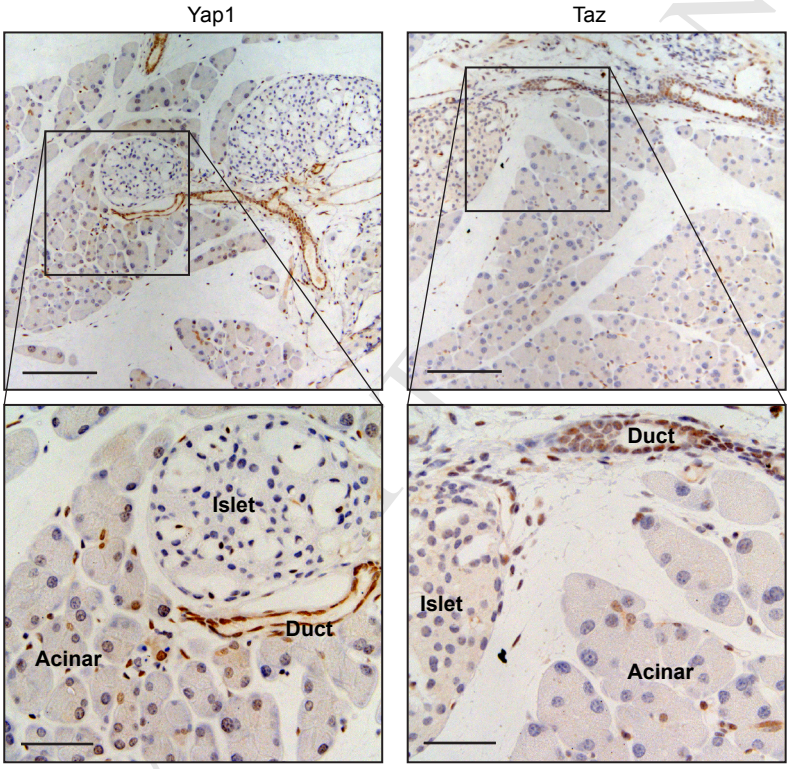

Supplementary Figure 1. Gene set enrichment analysis of caerulein-treated mice, and YAP1/TAZ localization in untreated pancreas. (A) Table of gene sets identified by gene set enrichment analysis of data set generated by Ulmasov et al. [6]. Gene signatures significantly enriched (nominal (NOM) *P*-value <.05) are shown and ranked by normalized enrichment score. YAP1 gene signatures are highlighted in red and IL6-STAT3 pathway signatures are highlighted in green. **(B)** Immunohistochemical stains with antibodies against YAP1 and TAZ in pancreata of C57BL/6 mice. Scale bars (top row) 200 µm; (bottom row) 50 µm.

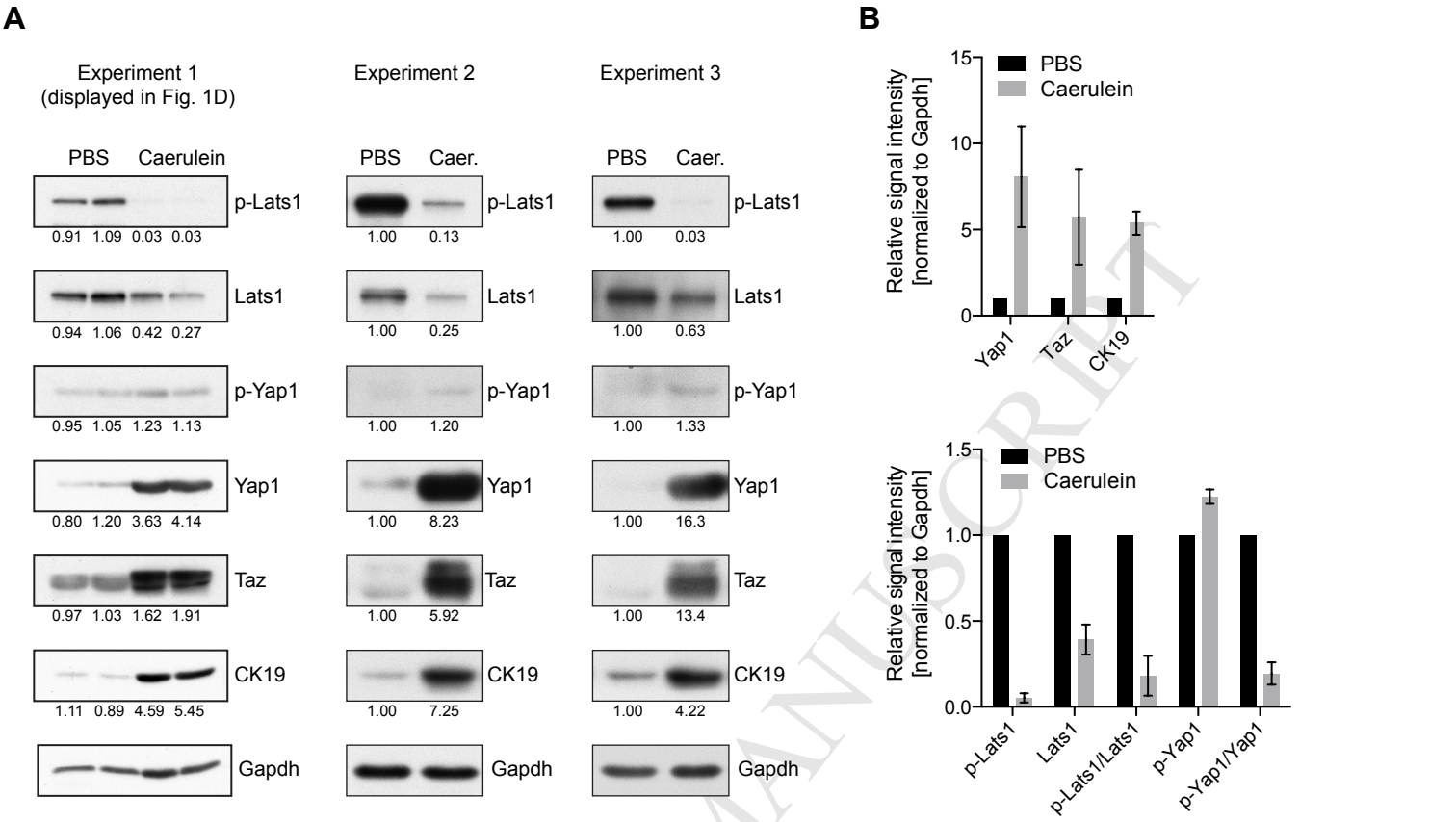

Supplementary Figure 2. (A) Immunoblots of phosphorylated Lats1 (Ser909), Lats1, phosphorylated YAP1 (Ser112), YAP1, TAZ, CK19 and Gapdh in pancreas lysates from caerulein- and PBS-treated animals from 3 independent experiments. Numbers under each blot represent band signal intensity normalized to Gapdh and relative to samples from PBS-treated animals. **(B)** Quantification of band signal intensity of immunoblots shown in (A); means ± SEM are shown.

ACCEPTED MANUSCRIPT

A

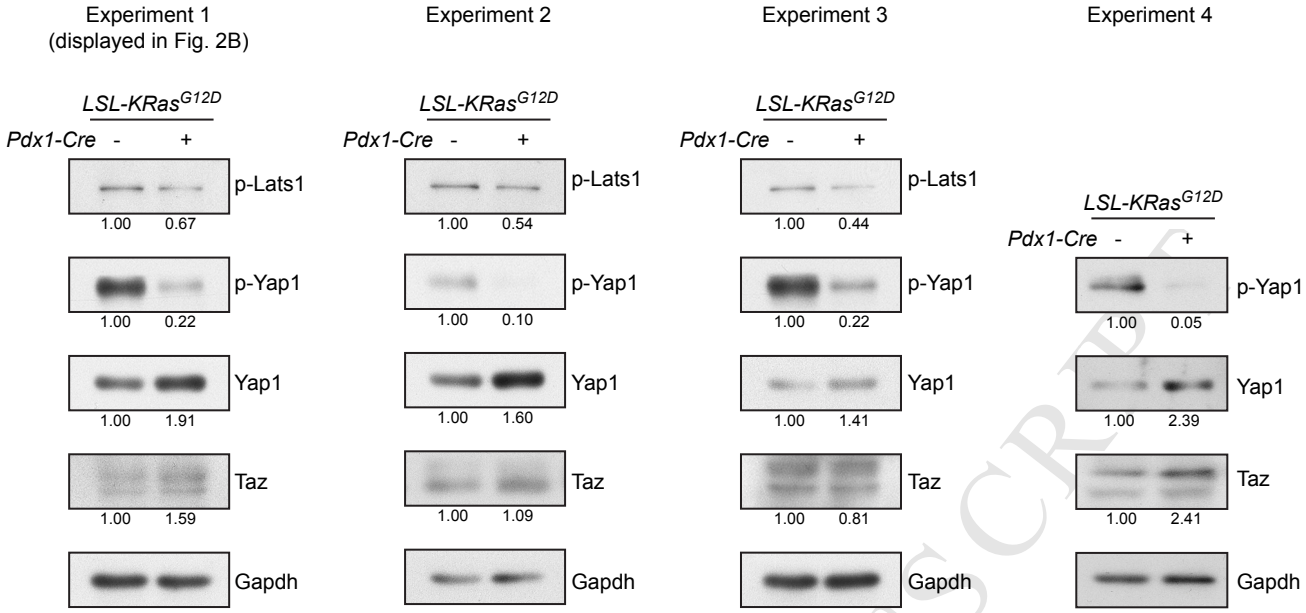

B

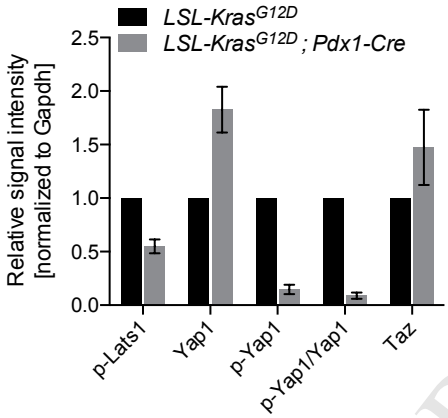

Supplementary Figure 3. (A) Immunoblots of phosphorylated Lats1 (Ser909), phosphorylated YAP1 (Ser112), YAP1, TAZ and Gapdh in pancreas lysates from control *LSL-KRas^{G12D}* and *LSL-KRas^{G12D};Pdx1-Cre* mice from 3-4 independent experiments. Numbers under each blot represent band signal intensity normalized to Gapdh and relative to samples from control *LSL-KRas^{G12D}* mice. **(B)** Quantification of band signal intensity of immunoblots shown in (A); means ± SEM are shown.

ACCEPTED MANUSCRIPT

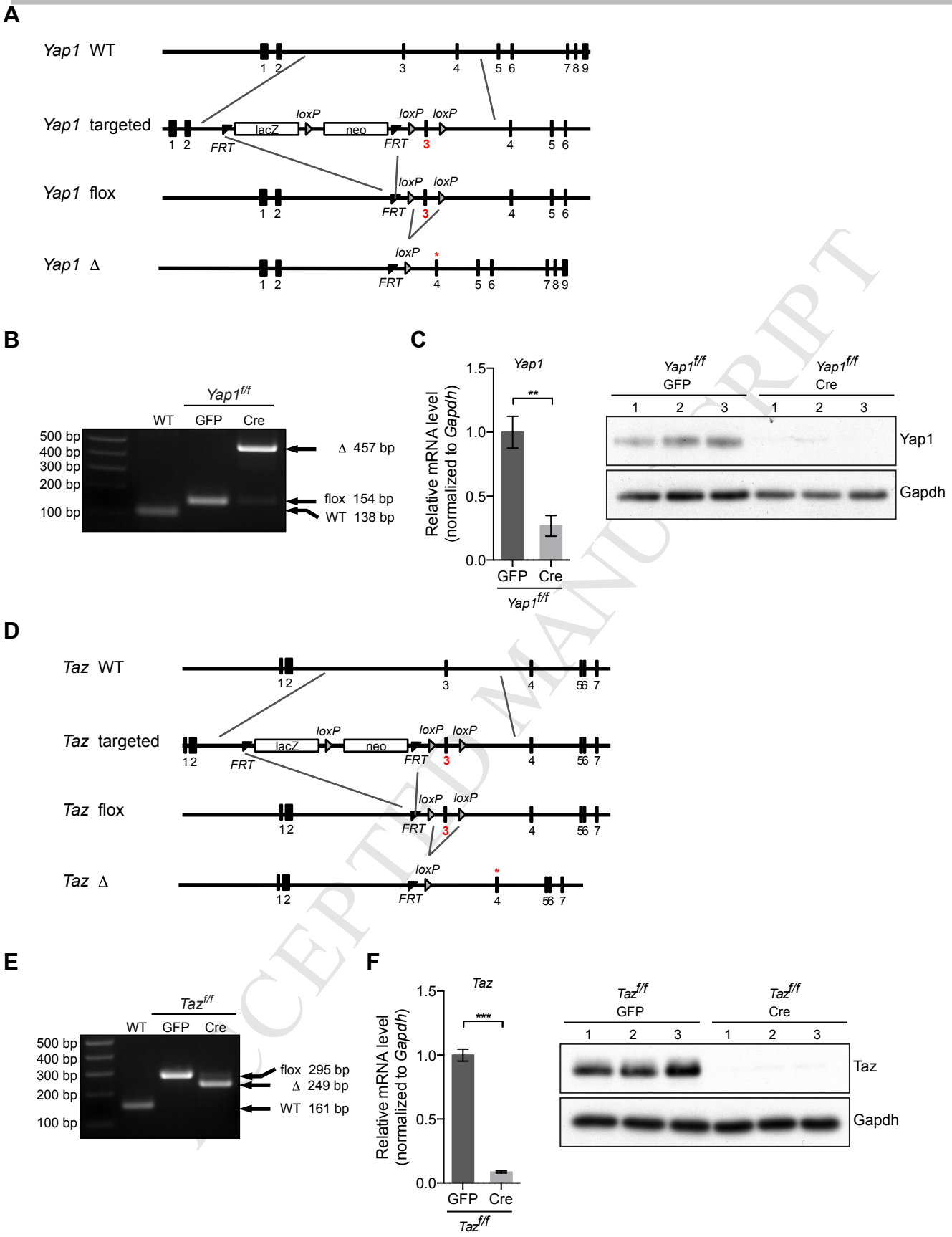

Supplementary Figure 4. Generation of conditional *Yap1* and *Taz* alleles. (A) Gene targeting strategy for conditional deletion of exon 3 in the mouse *Yap1* gene. Red asterisk indicates an induced stop codon by frame shift due to exon 3 deletion. **(B)** PCR genotyping of mouse embryonic fibroblasts (MEFs) isolated from WT or *Yap1*$^{f/f}$ embryos. Primary *Yap1*$^{f/f}$ MEFs were infected with either adenovirus-GFP (GFP) or adenovirus-Cre (Cre) and harvested 3 days later. **(C)** Quantitative RT-PCR analysis (left) and immunoblot analysis (right) of Yap1 in primary *Yap1*$^{f/f}$ MEFs infected with adenovirus-GFP (GFP) or adenovirus-Cre (Cre) 3 days after infection. Immunoblot analysis was performed with antibodies against Yap1 and Gapdh. n = 3 MEF clones isolated from 3 embryos; mean ± SEM is shown; ***P*<.01, Student's *t*-test. **(D)** Gene targeting strategy for conditional deletion of exon 3 in the mouse *Taz/Wwtr1* gene. Red asterisk indicates an induced stop codon by frame shift due to exon 3 deletion. **(E)** PCR genotyping of MEFs isolated from WT or *Taz*$^{f/f}$ embryos 3 days after infection with adenovirus-GFP (GFP) or adenovirus-Cre (Cre). **(F)** Quantitative RT-PCR analysis (left) and immunoblot analysis (right) of Taz in primary *Taz*$^{f/f}$ MEFs infected with adenovirus-GFP (GFP) or adenovirus-Cre (Cre), 3 days after infection. Immunoblot analysis was performed with antibodies against Taz and Gapdh. n = 3 MEF clones isolated from 3 embryos; mean ± SEM is shown; ***P*<.01, Student's *t*-test.

Gruber Supplementary Figure 5

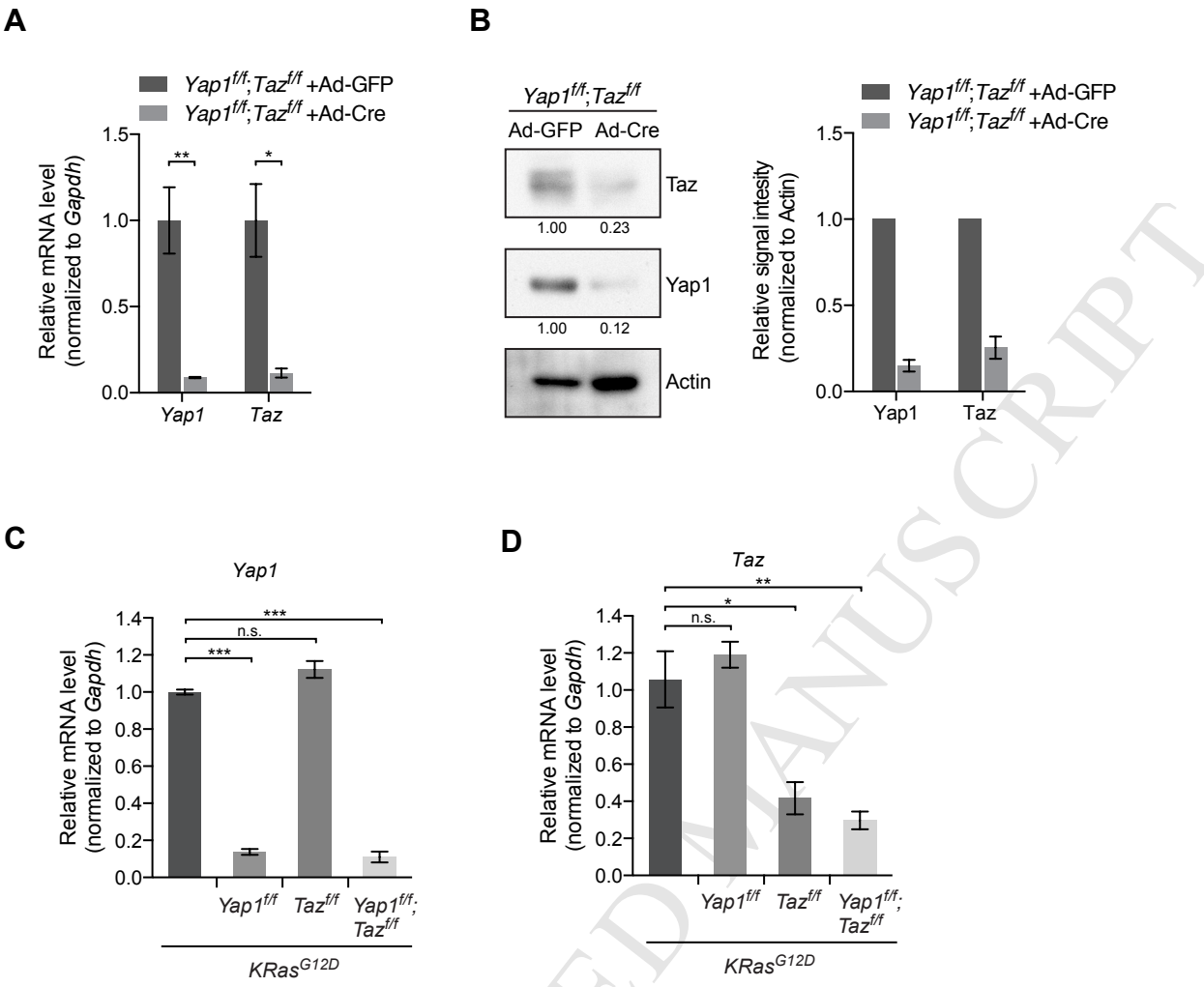

Supplementary Figure 5. Deletion efficiency of YAP1 and TAZ in primary acinar cells . (A) Quantitative RT-PCR of *Yap1* and *Taz* in primary acinar cells from *Yap1*$^{fl/fl}$;*Taz*$^{fl/fl}$ mice 3 days after isolation and infection with either adenovirus-GFP (Ad-GFP) adenovirus-Cre (Ad-Cre). n = 3 mice per group; mean ± SEM is shown; **P*<.05; ***P*<.01; Student's *t*-test. **(B)** Immunoblots of YAP1, TAZ and Actin in pancreas lysates from *Yap1*$^{fl/fl}$;*Taz*$^{fl/fl}$ mice 3 days after isolation and infection with either adenovirus-GFP (Ad-GFP) or adenovirus-Cre (Ad-Cre). Numbers under each blot represent band signal intensity normalized to Actin and relative to adenovirus-GFP infected cells. Graph shows quantification of band signal intensity of 3 independent experiments; means ± SEM are shown. **(C and D)** Quantitative RT-PCR of *Yap1* (A) and *Taz* (B) in primary acinar cells from *LSL-KRas*^{G12D}, *LSL-KRas*^{G12D};*Yap1*$^{fl/fl}$, *LSL-KRas*^{G12D};*Taz*$^{fl/fl}$ and *LSL-KRas*^{G12D};*Yap1*$^{fl/fl}$;*Taz*$^{fl/fl}$ mice 3 days after isolation and infection with adenovirus-Cre. n = 3 mice per group; mean ± SEM is shown; **P*<.05; ***P*<.01; ****P*<.005; n.s. = not significant, Student's *t*-test.

ACCEPTED MANUSCRIPT

Gruber Supplementary Figure 6

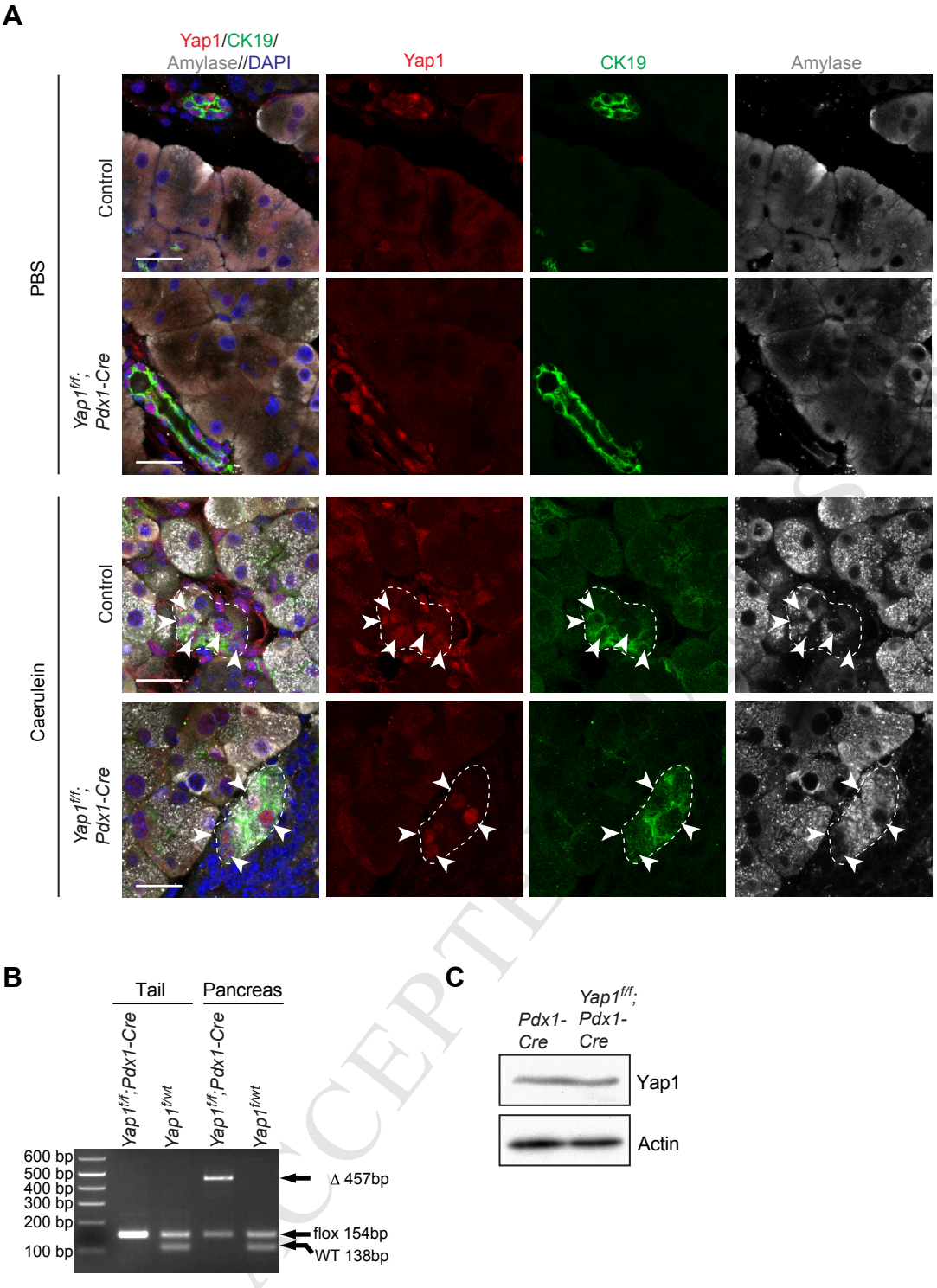

ACCEPTED MANUSCRIPT

Supplementary Figure 6. Evaluation of ADM and *Yap1* recombination in the *Pdx1-Cre* model. (A) Triple immunofluorescence of pancreata from control and *Yap1*$^{fl/fl}$*;Pdx1-Cre* mice, 4 days after PBS or caerulein treatment, with antibodies against CK19, amylase and YAP1. Scale bars = 20 µm. Arrowheads indicate ADM cells. **(B)** PCR genotyping of tail and pancreas DNA isolated from *Yap1*$^{f/wt}$ and *Yap1*$^{f/f}$*;Pdx1-Cre* mice. **(C)** Immunoblot analysis of pancreas lysates from *Pdx1-Cre* and *Yap1*$^{f/f}$*;Pdx1-Cre* mice with Yap1 and Actin antibodies.

Gruber Supplementary Figure 7

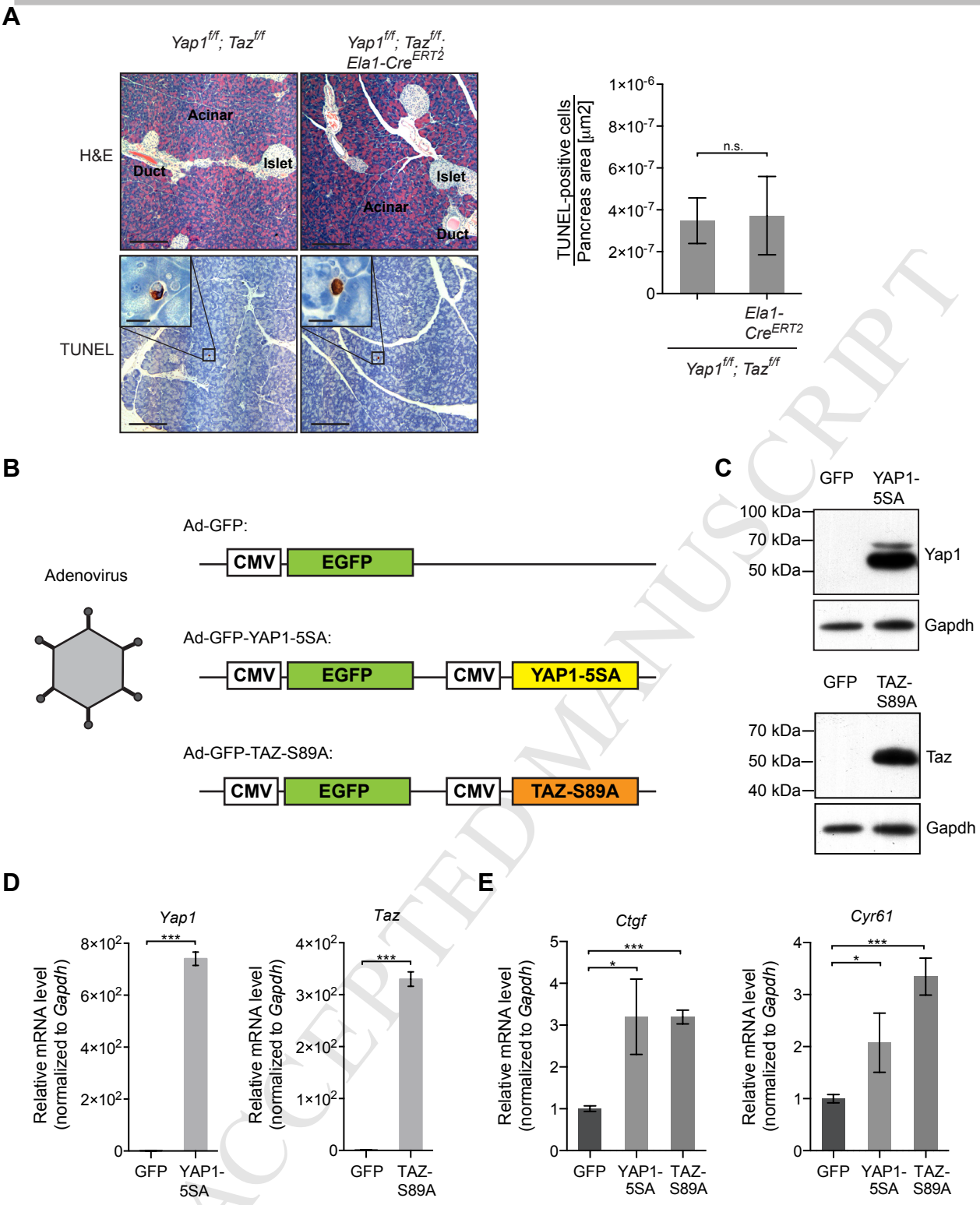

Supplementary Figure 7. TUNEL staining of YAP1/TAZ-deleted pancreas and validation of YAP1/TAZ-expressing adenoviruses. (A) H&E staining, TUNEL staining and quantification showing no increase in TUNEL staining in pancreatic sections from *Yap1*$^{f/f}$;*Taz*$^{f/f}$;*Ela1-Cre*^{ERT2} mice compared with *Yap1*$^{f/f}$;*Taz*$^{f/f}$ mice. Inset pictures show examples of TUNEL-positive cells. Scale bars = 200 µm; insets 20 µm. n = 3 mice per group; mean ± SEM is shown; n.s. = not significant, Student's *t*-test.**(B)** Schematic diagram of adenovirus constructs produced in the pAd-Track-CMV vector. **(C)** Immunoblot analysis of Gapdh and Yap1 or Taz in primary acinar cells 2 days after isolation and infection with adenovirus-GFP or adenovirus-GFP-YAP1-5SA or adenovirus-GFP-TAZ-S89A. **(D)** Quantitative RT-PCR analysis of *Yap1* or *Taz* in primary acinar cells 2 days after isolation and infection with adenovirus-GFP or adenovirus-GFP-YAP1-5SA or adenovirus-GFP-TAZ-S89A. n = 3-6 experiments; means ± SEM are shown; ***P<.005, Student's *t*-test. **(E)** Quantitative RT-PCR of the YAP1/TAZ target genes *Ctgf* and *Cyr61* in primary acinar cells 2 days after isolation. Acinar cells were infected with adenovirus encoding either GFP (Ad-GFP), GFP with YAP1-5SA (Ad-YAP1-5SA) or GFP with TAZ-S89A (Ad-TAZ-S89A) on the day of the isolation (day 0). n = 3-6 experiments; means ± SEM are shown; *P<.05; ***P<.005, Student's *t*-test.

ACCEPTED MANUSCRIPT

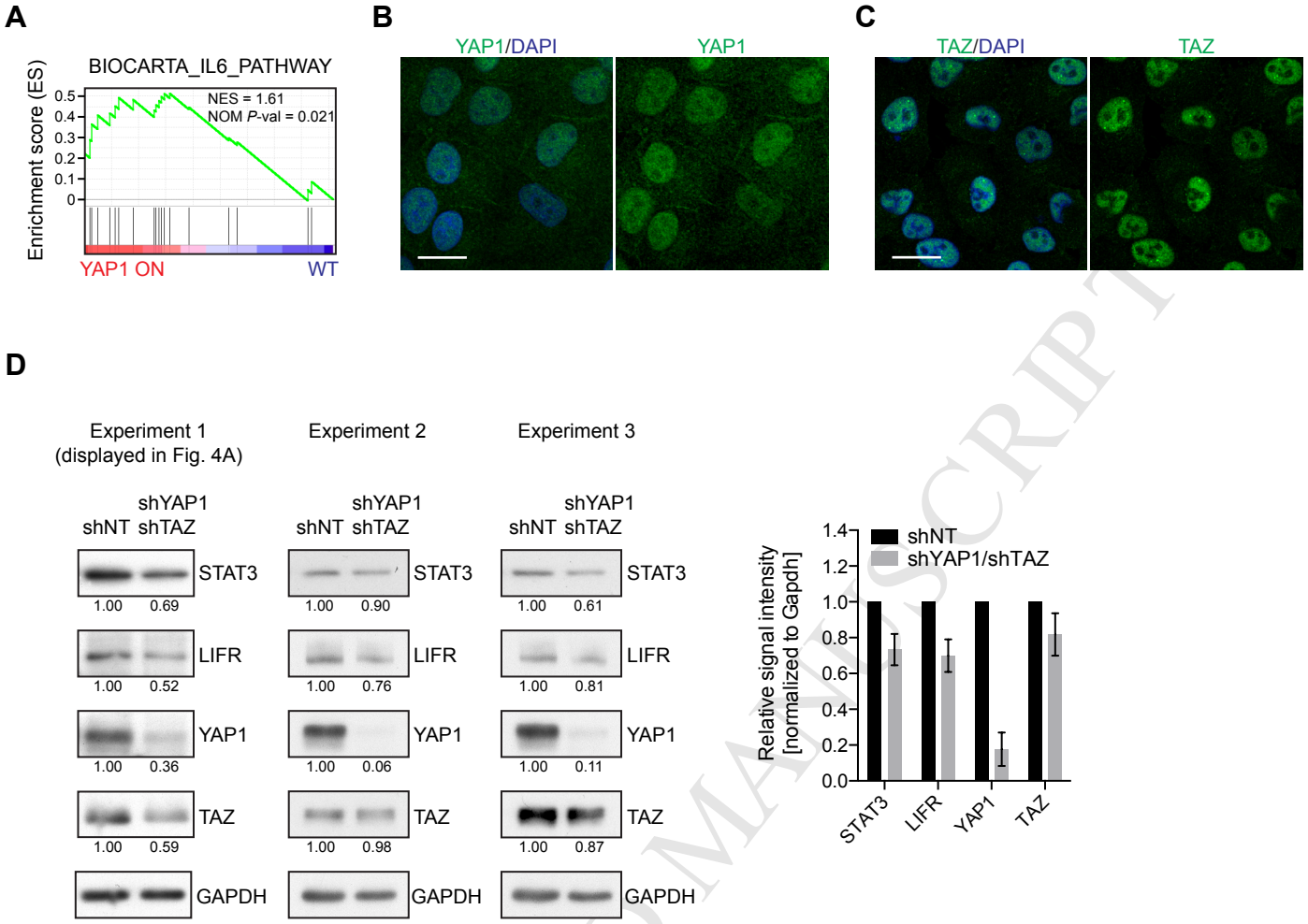

Supplementary Figure 8. YAP1/TAZ are active in PANC1 cells and knockdown of *YAP1*/*TAZ* results in reduced STAT3 and LIFR protein levels. (A) Gene set enrichment analysis of mouse liver organoids overexpressing YAP1 [7] identified the BIOCARTA annotated IL6 pathway [27, 28]. Normalized enrichment score (NES) and nominal (NOM) *P*-value are shown. **(B and C)** Immunofluorescence staining of PANC1 cells with Yap1 (B) or Taz (C) antibodies shows nuclear accumulation, indicating constitutive activation of YAP1/TAZ. Scale bars = 20 µm. **(D)** Immunoblots of STAT3, LIFR, YAP1, TAZ and GAPDH in lysates from PANC1 cells expressing shRNAs against YAP1 and TAZ or non-targeted shRNA control (shNT) from 3 independent experiments. Numbers under each blot represent band signal intensity normalized to GAPDH and relative to control shNT cells. Graph represents quantification of band signal intensity; means ± SEM are shown.

ACCEPTED MANUSCRIPT

Gruber Supplementary Figure 9

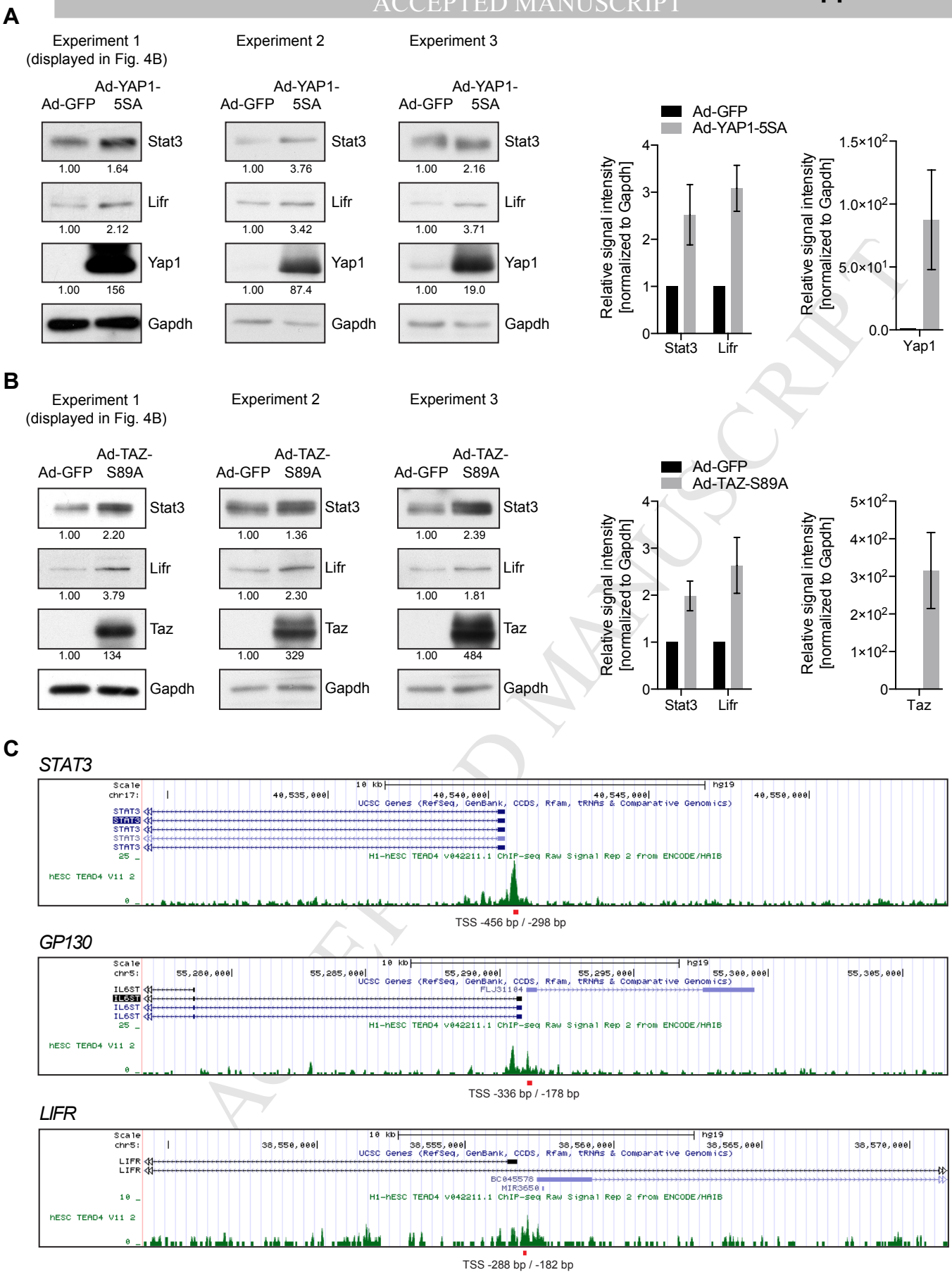

Supplementary Figure 9. Overexpression of active YAP1 and TAZ leads to increased STAT3 and LIFR protein levels and ENCODE dataset indicates peak for TEAD4 binding at the *STAT3*, *LIFR* and *GP130* promoters. (A and B). Immunoblots of primary acinar cell lysates 2 days after isolation and infection with Ad-GFP, Ad-YAP1-5SA-GFP (A) or Ad-TAZ-S89A-GFP (B) from 3 independent experiments. Numbers under each blot represent band signal intensity normalized to Gapdh and relative to control Ad-GFP infected cells. Graphs represent quantification of band signal intensity; means ± SEM are shown. **(C)** USCS Genome Browser view of TEAD4 ChIP-seq tracks from the ENCODE data set for human H1-hES cells. *STAT3*, *GP130* and *LIFR* loci are shown. PCR amplicons used for quantitative ChIP assay are indicated in red with their positions relative to transcription start sites (TSS).

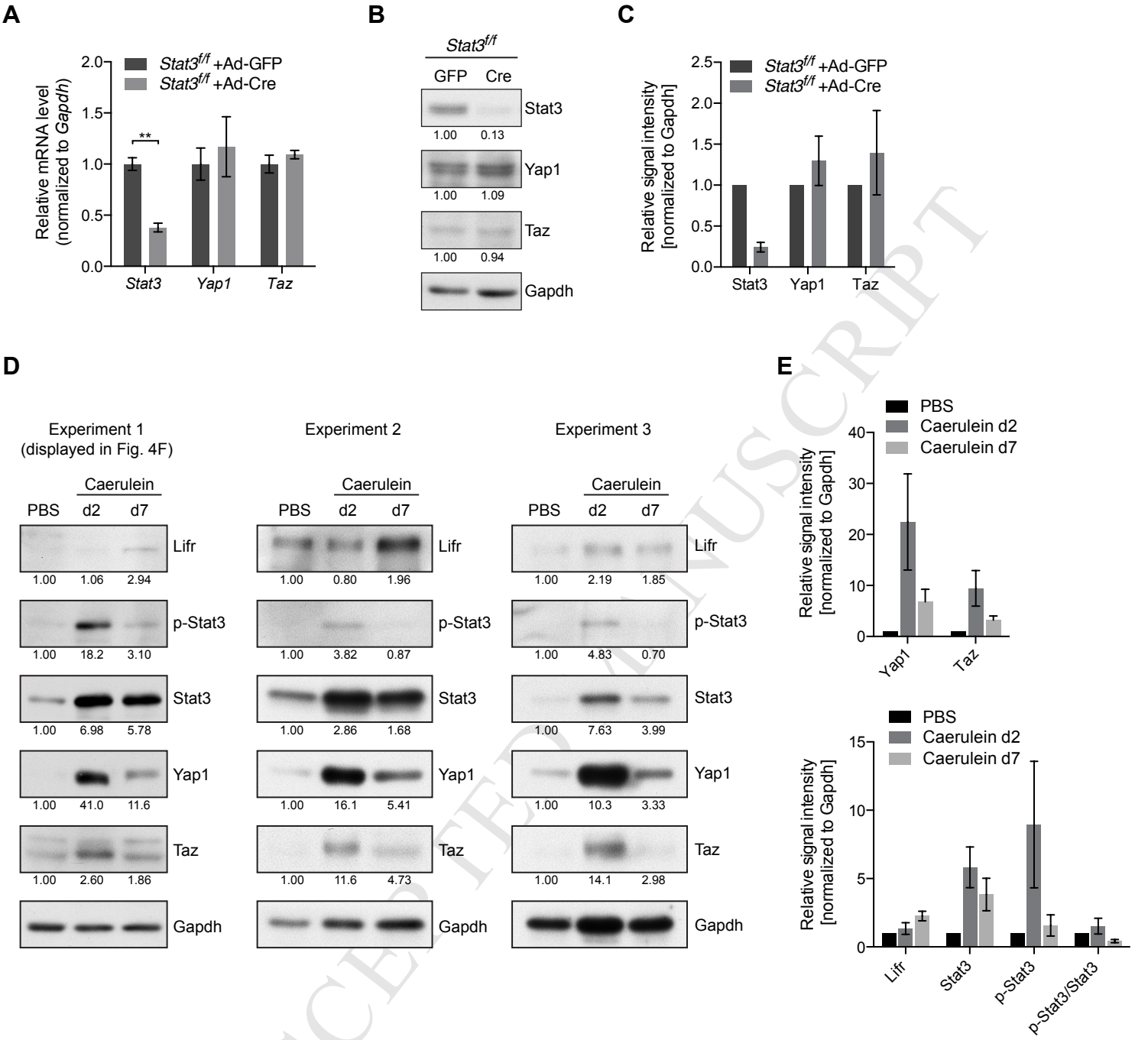

Supplementary Figure 10. STAT3 deletion in acinar cells has no effect on YAP1 and TAZ expression and protein levels and STAT3 is activated in response to caerulein treatment. (A) Quantitative RT-PCR of *Stat3*, *Yap1* and *Taz* in primary acinar cells from *Stat3*$^{f/f}$ mice 3 days after isolation and infection with either adenovirus-GFP (Ad-GFP) adenovirus-Cre (Ad-Cre). n = 3 mice per group; mean ± SEM is shown; ***P*<.01; Student's *t*-test. **(B)** Immunoblots of Stat3, YAP1, TAZ and Gapdh in pancreas lysates from *Stat3*$^{f/f}$ mice 3 days after isolation and infection with either adenovirus-GFP (GFP) or adenovirus-Cre (Cre). Numbers under each blot represent band signal intensity normalized to Gapdh and relative to adenovirus-GFP infected cells. **(C)** Quantification of band signal intensity of 3 independent experiments shown in (B); means ± SEM are shown. **(D)** Immunoblots of Lifr, phosphorylated Stat3 (Tyr705), Stat3, YAP1, TAZ and Gapdh in pancreas lysates from PBS- and caerulein-treated animals on day 2 (d2) and day 7 (d7) after treatment from 3 independent experiments. Numbers under each blot represent band signal intensity normalized to Gapdh and relative to samples from PBS-treated animals. **(E)** Quantification of band signal intensity of immunoblots shown in (D); means ± SEM are shown.

ACCEPTED MANUSCRIPT

Gruber Supplementary Figure 11

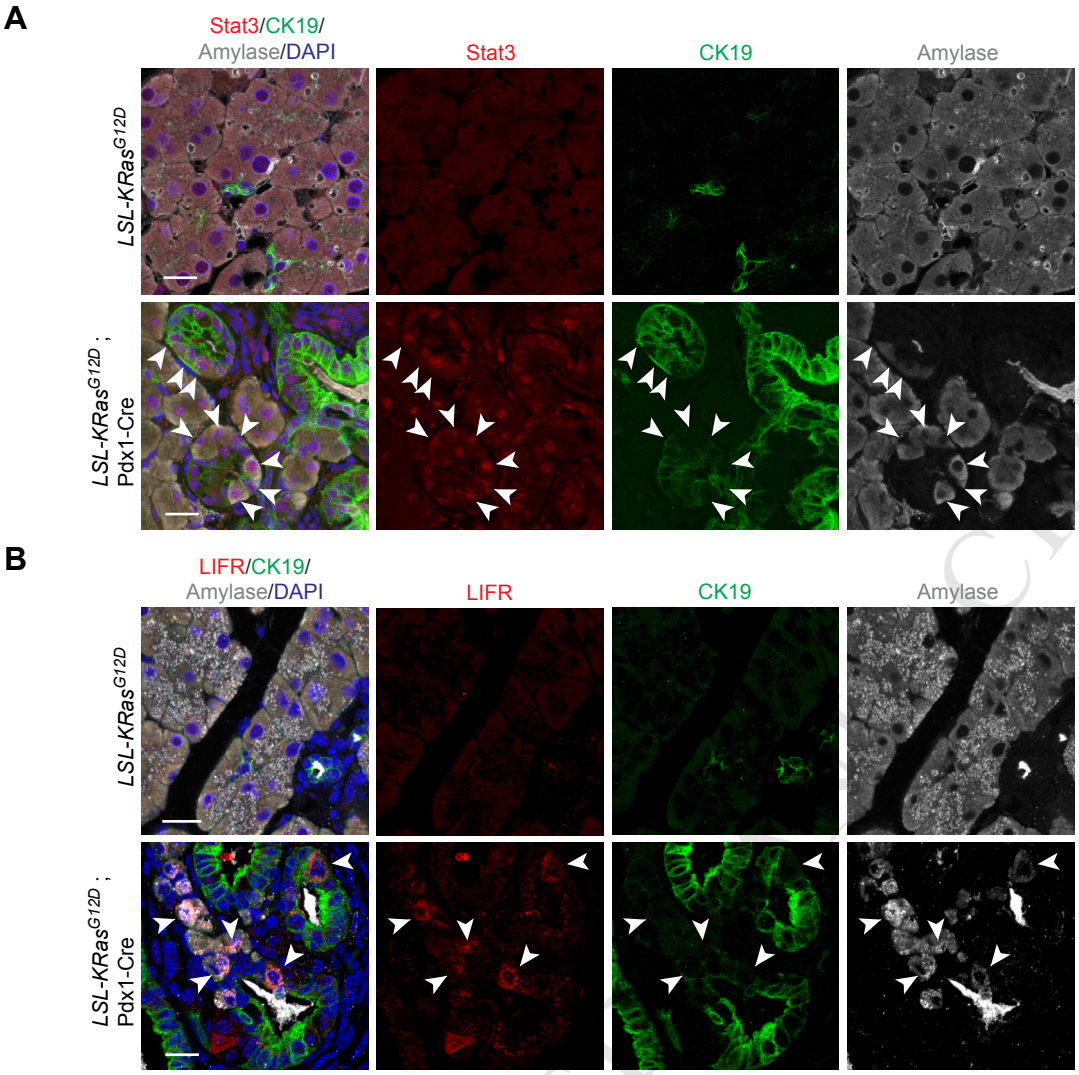

Supplementary Figure 11. STAT3 and LIFR are upregulated in ADM lesions. (A and B) Triple immunofluorescence of pancreata from *LSL-KRas^{G12D}* and *LSL-KRas^{G12D};Pdx1-Cre* mice with antibodies against the duct marker CK19, the acinar marker amylase and either STAT3 (A) or LIFR (B). Arrowheads indicate ADM cells. Scale bars = 20 µm.

ACCEPTED MANUSCRIPT

Gruber Supplementary Figure 12

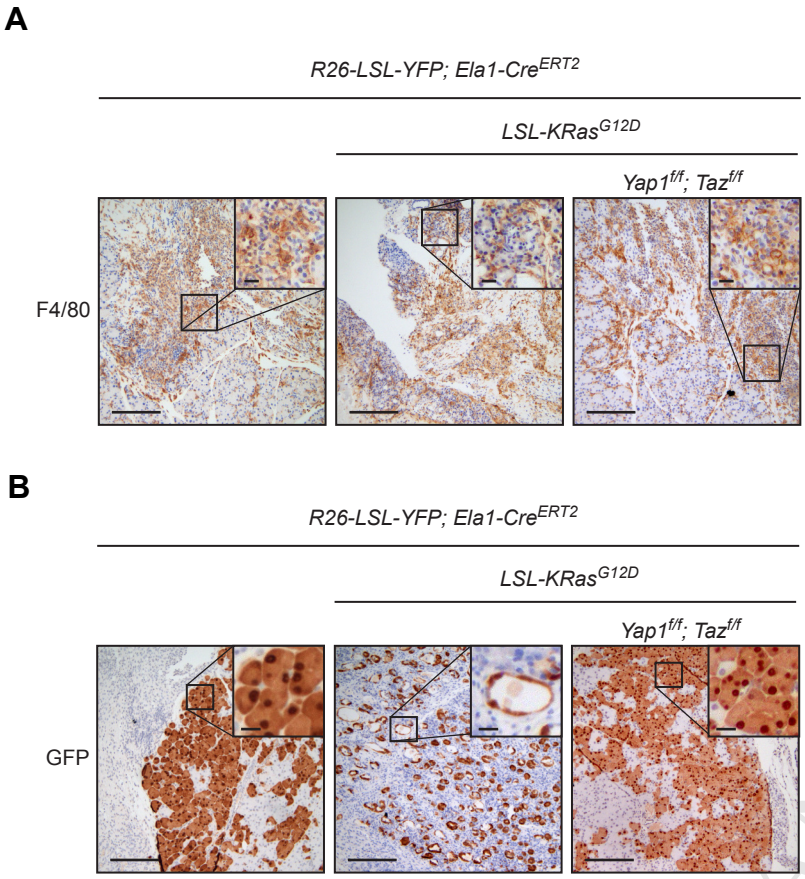

Supplementary Figure 12. Inflammation and lineage tracing in caerulein-treated pancreata. (A and B) Immunohistochemistry with antibodies against the macrophage marker F4/80 (A) or GFP (B) in pancreata from *R26-LSL-YFP;Ela1-Cre^{ERT2}*, *R26-LSL-YFP;LSL-KRas^{G12D};Ela1-Cre^{ERT2}*, and *R26-LSL-YFP;LSL-KRas^{G12D};Yap1$^{fl/fl}$;Taz$^{fl/fl}$;Ela1-Cre^{ERT2}* mice. Mice were injected 5 times with tamoxifen and treated with caerulein one week later as indicated in Figure 5A. Inset pictures show examples of F4/80-positive cells (A) and GFP-positive cells (B) at higher magnification. Scale bars = 200 μm; insets 20 μm.

ACCEPTED MANUSCRIPT

Gruber Supplementary Figure 13

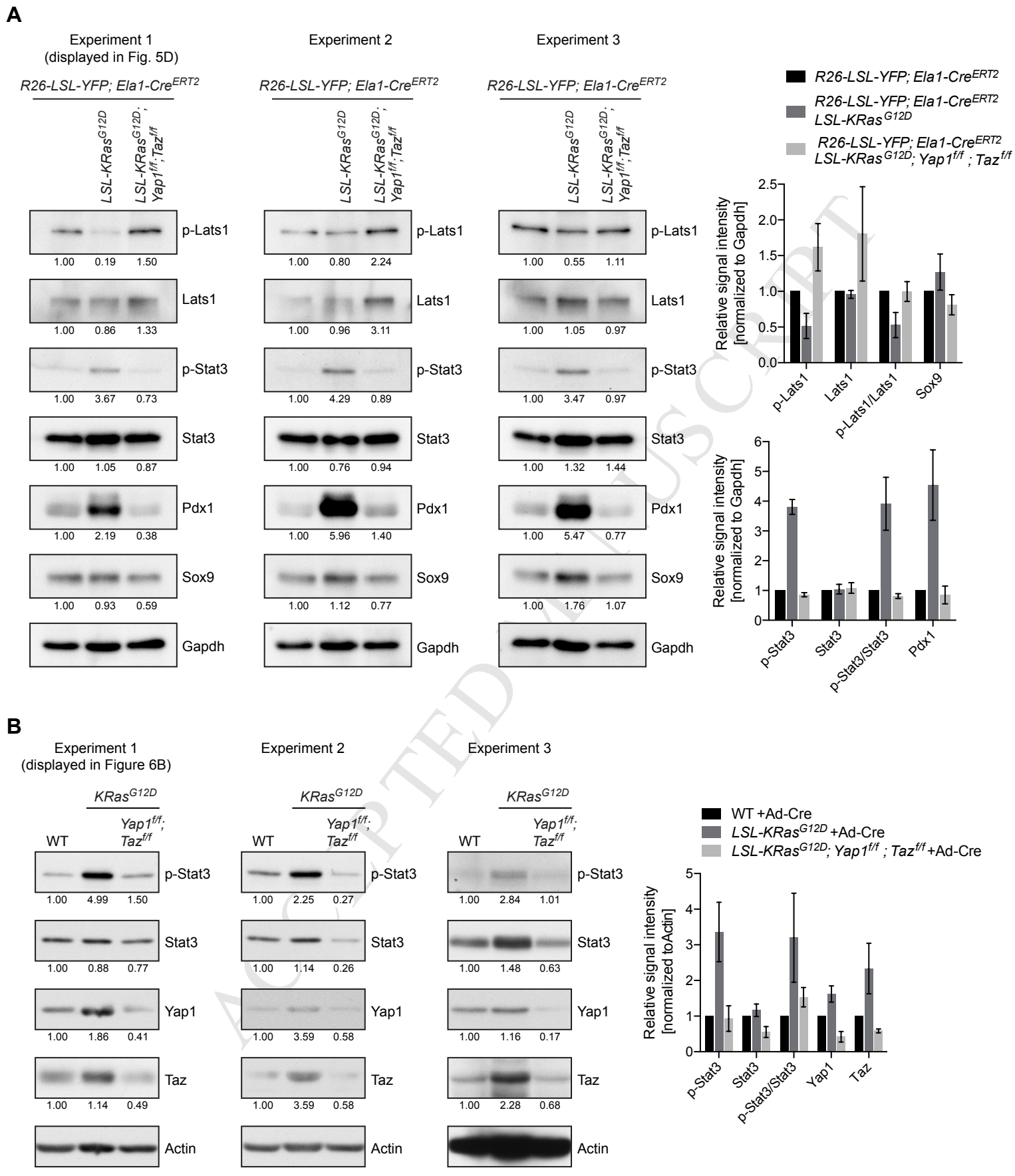

Supplementary Figure 13. (A) Immunoblots and quantification of band signal intensities of phosphorylated Lats1 (Ser909), Lats1, phosphorylated Stat3 (Tyr705), Stat3, Pdx1, Sox9 and Gapdh in pancreas lysates from caerulein-treated *R26-LSL-YFP;Ela1-Cre^{ERT2}*, *R26-LSL-YFP;LSL-KRas^{G12D};Ela1-Cre^{ERT2}*, and *R26-LSL-YFP;LSL-KRas^{G12D};Yap1$^{f/f}$;Taz$^{f/f}$;Ela1-Cre^{ERT2}* mice. Mice were injected 5 times with tamoxifen and treated with caerulein one week later as indicated in Figure 5A. Numbers under each blot represent band signal intensity normalized to Gapdh and relative to *R26-LSL-YFP;Ela1-Cre^{ERT2}* mice; means ± SEM are shown. **(B)** Immunoblots and quantification of band signal intensity of immunoblots from WT, *LSL-KRas^{G12D}* and *LSL-KRas^{G12D};Yap1$^{f/f}$;Taz$^{f/f}$* primary acinar lysates 2 days after isolation and adenovirus-Cre infection. Immunoblots of phosphorylated Stat3 (Tyr705), Stat3, Yap1, Taz and Actin are shown. Numbers under each blot represent band signal intensity normalized to Actin and relative to WT cells; means ± SEM are shown.

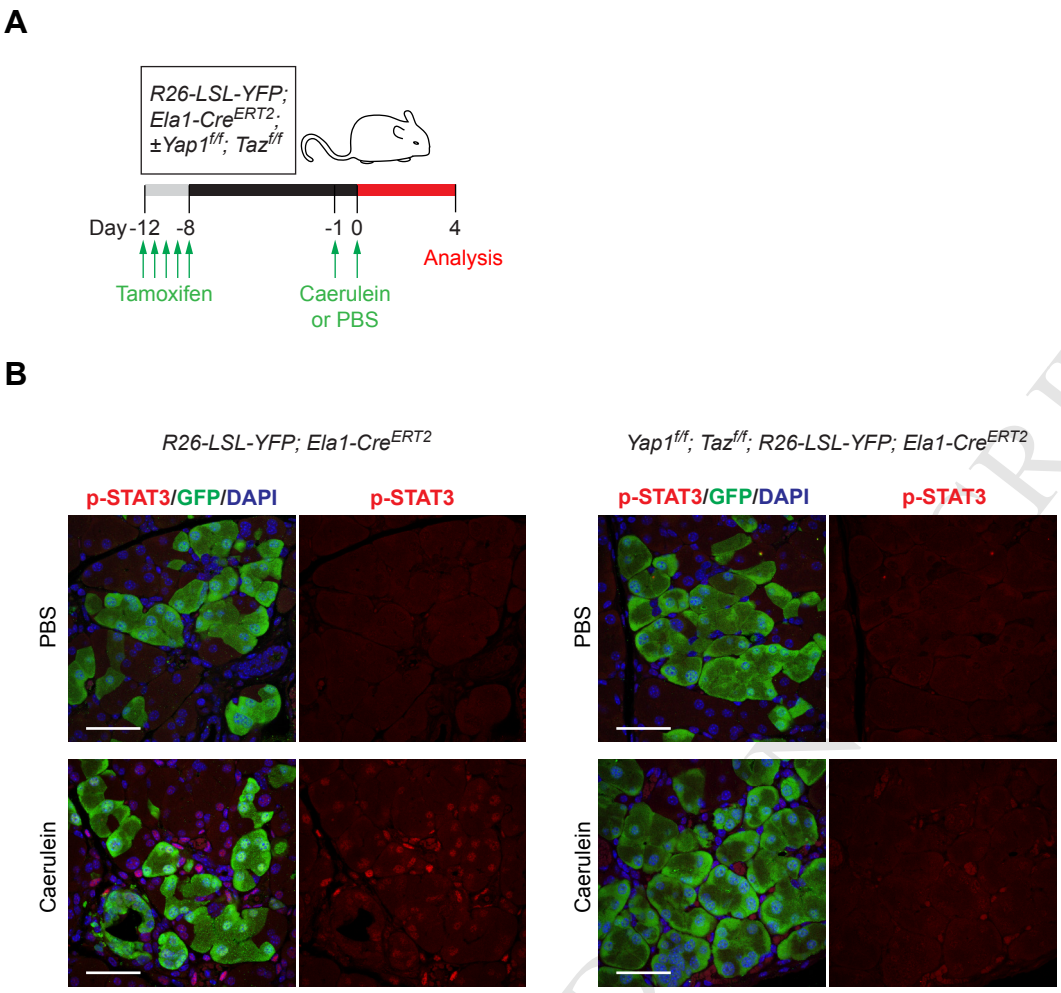

Supplementary Figure 14. Caerulein-mediated activation of STAT3 depends on YAP1 and TAZ. (A) Scheme showing experimental design of caerulein-induced acute pancreatitis in the acinar-specific and tamoxifen-inducible *Ela1-CreERT2* mouse model combined with the *R26-LSL-YFP* lineage tracer. **(B)** Double immunofluorescence of pancreata from *R26-LSL-YFP;Ela1-CreERT2* and *Yap1f/f;Taz f/f;R26-LSL-YFP;Ela1-CreERT2* mice with antibodies against GFP, labeling recombined cells, and phosphorylated Stat3 (Tyr705). Mice were treated with tamoxifen and with either PBS or caerulein as indicated in (A). Scale bars = 50 µm.

ACCEPTED MANUSCRIPT

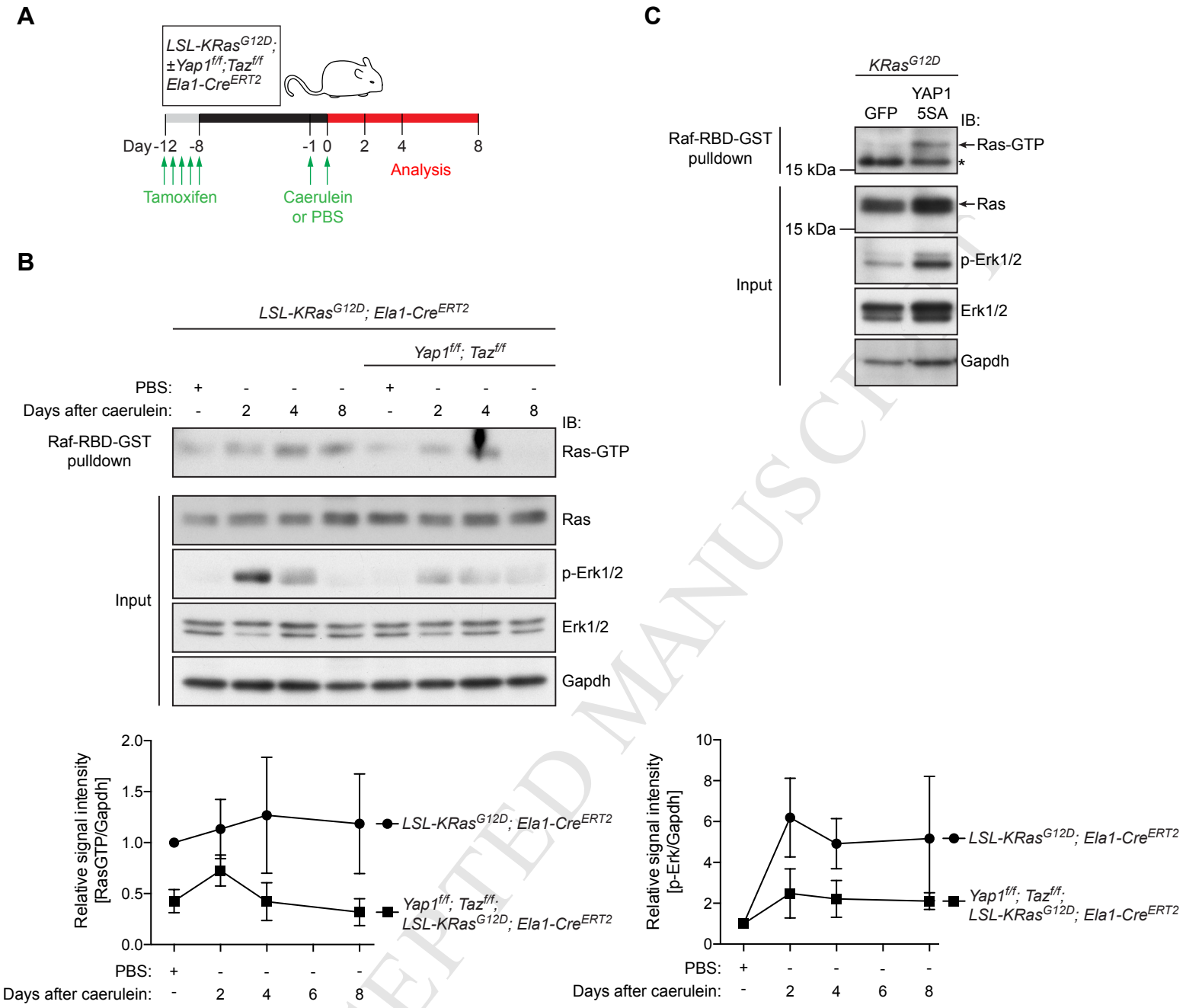

Supplementary Figure 15. Deletion of YAP1 and TAZ reduced the caerulein-induced increase in Ras activity. (A) Scheme showing experimental design of caerulein-induced acute pancreatitis in cooperation with acinar-specific tamoxifen-inducible *KRas^{G12D}* mutation. **(B)** Immunoblots (IB) of pancreas lysates from *LSL-KRas^{G12D};Ela1-Cre^{ERT2}* and *Yap1$^{f/f}$;Taz$^{f/f}$;LSL-KRas^{G12D};Ela1-Cre^{ERT2}* mice treated with tamoxifen and either PBS or caerulein as indicated in (A). Antibodies against Ras, phosphorylated p-Erk1/2 (Thr202/Tyr204), Erk1/2 and Gapdh were used. Ras-GTP levels were determined with an active Ras pull-down assay using the Ras-binding-domain from Raf fused to GST (Raf-RBD-GST). Representative immunoblots are shown and graphs show quantification of band signal intensity of Ras-GTP normalized to Gapdh and relative to control PBS-treated *LSL-KRas^{G12D};Ela1-Cre^{ERT2}* mice (left graph) and band signal intensity of phosphorylated p-Erk1/2 (Thr202/Tyr204) normalized to Gapdh and relative to control PBS-treated mice (right graph) from 3-4 independent experiments; means ± SEM are shown. **(C)** Immunoblots (IB) of primary acinar cells from *LSL-KRas^{G12D}* mice, 3 days after isolation and infection with adenovirus-Cre together with either adenovirus-GFP (GFP) or adenovirus-YAP1-5SA (YAP1-5SA), with antibodies against Ras, phosphorylated p-Erk1/2 (Thr202/Tyr204), Erk1/2 and Gapdh. Ras-GTP levels were determined with an active Ras pull-down assay using the Ras-binding-domain from Raf fused to GST (Raf-RBD-GST). Asterisks indicate non-specific bands.

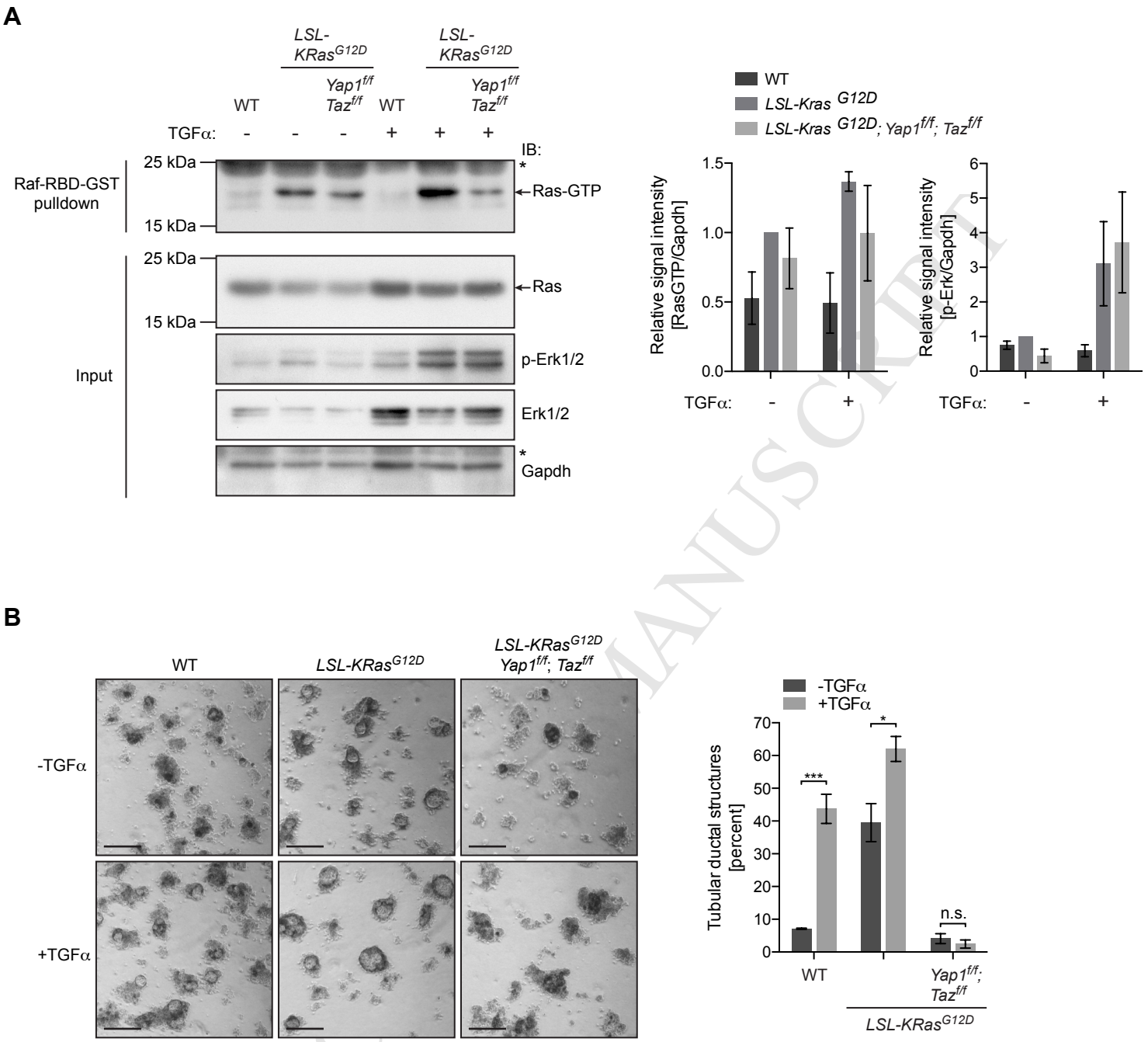

Supplementary Figure 16. YAP1 and TAZ are required for ADM after TGFα-induced increase in oncogenic Ras activity. (A) Immunoblots (IB) of primary acinar cells from WT, *LSL-KRas^{G12D}* and *LSL-KRas^{G12D};Yap1$^{f/f}$;Taz$^{f/f}$* mice 3 days after isolation and adenovirus-Cre infection with antibodies against Ras, phosphorylated p-Erk1/2 (Thr202/Tyr204), Erk1/2 and Gapdh. Ras-GTP levels were determined with an active Ras pull-down assay using the Ras-binding-domain from Raf fused to GST (Raf-RBD-GST). Cells were either untreated or treated with TGFα (50 ng/ml) for 3 days. Asterisks indicate non-specific bands. Representative immunoblots are shown and graphs show quantification of band signal intensity from 3 independent experiments. Band signal intensities of Ras-GTP (left graph) or phosphorylated p-Erk1/2 (right graph) were normalized to Gapdh and are shown as relative to *LSL-KRas^{G12D}* mice without TGFα treatment; means ± SEM are shown. **(B)** Brightfield images of pancreatic acinar cell clusters on day 5 after isolation from WT, *LSL-KRas^{G12D}* and *LSL-KRas^{G12D};Yap1$^{f/f}$;Taz$^{f/f}$* mice. Cells were infected with adenovirus-Cre on day 0 and either untreated or treated with TGFα (50 ng/ml) from day 0 for 5 days. Scale bars = 100 µm. Graph shows quantification of tubular ductal structures of the indicated genotypes with n = 3 mice per group; means ± SEM are shown; ***P<.005, *P<.05, Student's t-test.

ACCEPTED MANUSCRIPT

Supplementary Table 1. List of primers for quantitative RT-PCR

Species	Gene	Primer	Sequence
Human	*GAPDH*	forward reverse	5'-AGCCACATCGCTCAGACAC-3' 5'-GCCCAATACGACCAAATCC-3'
Human	*YAP1*	forward reverse	5'-CCCAGATGAACGTCACAGC-3' 5'-GATTCTCTGGTTCATGGCTGA-3'
Human	*TAZ*	forward reverse	5'-ATCCCAGCCAAATCTCGTGA-3' 5'-GCCCTGCGGGTGGGT-3'
Human	*ANKRD1*	forward reverse	5'-AACGGAAAAGCGAGAAACTG-3' 5'-TTCAAGCTTTGATCTTTGTTCTAGTT-3'
Human	*AMOTL2*	forward reverse	5'-AGGCTGCAGAGAGACAATGAG-3' 5'-CTCAGAGAGCCGCTGGATT-3'
Human	*STAT3*	forward reverse	5'-CCCTTGGATTGAGAGTCAAGA-3' 5'-AAGCGGCTATACTGCTGGTC-3'
Human	*LIR*	forward reverse	5'-GAGTATGTATGTGGTGACAAAGGAA-3' 5'-TCACCACTCCAACAATGACAG-3'
Human	*GP130*	forward reverse	5'-AGGACCAAAGATGCCTCAAC-3' 5'-GAATGAAGATCGGGTGGATG-3'
Human	*IL13RA1*	forward reverse	5'-GTGCCTTTAACTTCCCGTGT-3' 5'-CCCATTGCACATATAGGTCATC-3'
Human	*JAK1*	forward reverse	5'-CTGGAGTATCTGTTTGCTCAGG-3' 5'-GCTCGGTCTTGGGGTCTC-3'
Mouse	*Gapdh*	forward reverse	5'-TGTCCGTCGTGGATCTGAC-3' 5'-CCTGCTTCACCACCTTCTTG-3'
Mouse	*Yap1*	forward reverse	5'-GTCCTCCTTTGAGATCCCTGA-3' 5'-TGTTGTTGTCTGATCGTTGTGAT-3'
Mouse	*Taz*	forward reverse	5'-TGCTACAGTGTCCCCACAAC-3' 5'-TGACCGGAATTTTCACCTGT-3'
Mouse	*Ctgf*	forward reverse	5'-GTGCCAGAACGCACACTG-3' 5'-CCCCGGTTACACTCCAAA-3'

Mouse	*Cyr61*	forward reverse	5'-GGATCTGTGAAGTGCGTCC-3' 5'-CTGCATTTCTTGCCCTTTTT-3'
Mouse	*Ankrd1*	forward reverse	5'-AACGGAAAAGCGAGAAACTG-3' 5'-TTCAAGCTTTGATCTTTGTTCTAGTT-3'
Mouse	*Amotl2*	forward reverse	5'-TGACTGTACCTAAGCCGAACC-3' 5'-GCACACACCTGCCTAGACAAT-3'
Mouse	*Stat3*	forward reverse	5'-GTTCCTGGCACCTTGGATT-3' 5'-CAACGTGGCATGTGACTCTT-3'
Mouse	*Lifr*	forward reverse	5'-TGTTTGTGGTGACCAAGGAA-3' 5'-TTACCACGCCAACAATGACA-3'
Mouse	*Gp130*	forward reverse	5'-GACCCGATAGAAGGAACATGAC-3' 5'-TGGTGCTGACATCTTGCAG-3'
Mouse	*Jak1*	forward reverse	5'-GGAGTACTACACAGTCAAGGACGA-3' 5'-AAACATTCCGGAGCGTACC-3'

ACCEPTED MANUSCRIPT

ACCEPTED MANUSCRIPT

Supplementary Table 2. List of primers for quantitative ChIP analysis

Species	Gene	Primer	Sequence
Human	*ZFP37 intron*	forward reverse	5'- ACCATGCCCAGCTACGTTTTGT -3' 5'- AGGATTGCTTGAGCTCAGGAGT -3'
Human	*CTGF promoter*	forward reverse	5'- TTCAGACGGAGGAATGCTGAGTGT -3' 5'- CCAATGAGCTGAATGGAGTCCTAC -3'
Human	*STAT3 promoter*	forward reverse	5'- TCACGCACTGCCAGGAACTCA -3' 5'- GTGCTGGCTGTTCCGACAGTT -3'
Human	*STAT3 intron*	forward reverse	5'- AGTGCTGGGATTACAGGCATGA -3' 5'- GTTTGTGTTGGGGATAGCCCATGA -3'
Human	*LIFR promoter*	forward reverse	5'- GAAGGTTAGATTGGCCCCATGGAT -3' 5'- AAGCTTTTGCCTCCAGGCCA -3'
Human	*LIFR intron*	forward reverse	5'- TTGCAGGACTTCTGAGAGCCTT -3' 5'- GAGGGGAGTCTATGTATGGTCAGT -3'
Human	*GP130 promoter*	forward reverse	5'- GCTCCAGTTCATGACCCCGTTATT -3' 5'- ATTCCCGTAACGCGGCTCTT -3'
Human	*GP130 intron*	forward reverse	5'- GTGAAAGGCTTCAGAAACACTTG -3' 5'- AGATACACTAGATAGCCGCAAAG -3'

ACCEPTED MANUSCRIPT

ACCEPTED MANUSCRIPT

Supplementary Materials and Methods

Mouse Lines

For genotyping of the *Yap1* and *Taz* conditional alleles, genomic DNA from ear snips, cells or tissues was used with PCR primers for *Yap1*: Yap1-f 5'-GCTTCCTGTAGTCATGTGGTTGT-3', Yap1-r 5'-TGTTGTCATATGCCATTGTGTAA-3' and Yap1-delta-f 5'-CACAGAGATCCTCCTGTCTCAG-3' producing PCR bands of 138 bp (wildtype), 154 bp (floxed) and 457 bp (deleted). PCR primers used for *Taz*/*Wwtr1* genotyping were Taz-f 5'-AGCAAAGTAAGGGCACTGTATG-3', Taz-r 5'-GCTCCCAAACCACATCACAG-3' and Taz-delta-r 5'-TCTACTCTTGGCTCTTAGCTGG-3' producing PCR bands of 161 bp (wildtype), 295 bp (floxed) and 249 bp (deleted). See diagrams in **Supplementary Fig 4A and D** for allele details and **Supplementary Fig 4B,C and 4E,F** for validation of the knock-out alleles in $Yap1^{fl/fl}$ and $Taz^{fl/fl}$ primary MEFs isolated from E13.5 embryos.

Previously described mouse lines used were $Stat3^{fl/fl}$ [1], *Pdx1-Cre* [2], *R26-LSL-YFP* [3], *LSL-KRas*^{G12D} [4] and *Ela1-Cre*^{ERT2} [5].

These lines were intercrossed to obtain the different genotypes. In order to maintain a similar genetic background in the knock-out and control groups, mice carrying the *R26-LSL-YFP*, *LSL-KRas*^{G12D} and *Ela1-Cre*^{ERT2} alleles were first crossed into the $Yap1^{fl/fl}$;$Taz^{fl/fl}$ or the $Stat3^{fl/fl}$ background. The resulting mice carrying the $Yap1^{fl/+}$ and $Taz^{fl/+}$ or the $Stat3^{fl/+}$ alleles together with the *R26-LSL-YFP*, *LSL-KRas*^{G12D} and *Ela1-Cre*^{ERT2} alleles were then intercrossed to breed out the floxed alleles (control groups) or to obtain the homozygous floxed alleles (knock-out groups). Controls for the *LSL-*

KRas^{G12D}*;Pdx1-Cre* mice were litter mates harbouring the *LSL-KRas*^{G12D} allele without the *Pdx1-Cre* transgene.

All mouse experiments were performed on sex- and age-matched adult mice at the age of 8-14 weeks and analysed at the indicated time points. The *LSL-KRas*^{G12D}*;Pdx1-Cre* and respective control mice were analysed at 6 months.

For the induction of recombination in pancreatic acinar cells using the *Ela1-Cre*^{ERT2} mouse line, adult mice (8-14 weeks) were injected intra-peritoneally with 100 μg/g body weight tamoxifen (Sigma-Aldrich) dissolved in peanut oil (Sigma-Aldrich) once daily for five consecutive days.

Cell lines

The pancreatic adenocarcinoma cell line PANC-1 and the rat acinar cell line AR42J were purchased from HPA Cultures and authenticated by Short Tandem Repeat (STR) profiling (Promega). PANC-1 cells were cultured in DMEM medium (Life technologies) containing 10 % fetal bovine serum (FBS) and Penicillin/Streptomycin (Sigma-Aldrich) and AR42J cells were cultured in RPMI medium (Life technologies) supplemented with 10 % FBS and Penicillin/Streptomycin (Sigma-Aldrich). All cell lines were passaged for a maximum of 6 months after authentication.

Immunofluorescence and immunohistochemistry staining

Mice were euthanized by cervical dislocation and the pancreas was dissected out and fixed overnight in 10 % neutral buffered formalin, then washed with 70 % ethanol, processed and embedded into paraffin. Sections were cut at a thickness of 4 μm and deparaffinized in Histo-Clear (National Diagnostics), rinsed in ethanol and washed in water and PBS. Sections were stained with Haematoxylin & Eosin (H&E) or with

antibodies for immunofluorescence or immunohistochemistry. Antigen retrieval was performed by incubating sections in 10 mM sodium citrate (pH 6) for 10 minutes at sub-boiling temperature and keeping them in the same buffer for 30 min before washing with PBS.

For immunohistochemistry, endogenous peroxidase was blocked with 3 % hydrogen peroxide for 5 min followed by washes with PBS. Epitope blocking was performed for 1 h at room temperature (RT) with blocking solution: 1 % bovine serum albumin (Sigma-Aldrich), 5 % normal donkey serum (Millipore) and 0.4 % Triton X-100 (Sigma-Aldrich) diluted in PBS. Sections were then incubated overnight at 4 ºC with primary antibodies diluted in blocking solution. Next day, sections were washed with PBS and incubated for 2 h at RT with secondary antibodies (Life Technologies) diluted in blocking solution, then washed again and staining was visualized with 3.3'-diaminobenzidine (DAB) followed by counterstaining with Mayer's hematoxylin. The sections were then dehydrated and mounted.

For immunofluorescence, epitope blocking, antibody and washing steps were performed as above except the secondary antibody solution contained DAPI at a concentration of 0.75 nM, and sections were stained with 0.1 % Sudan Black B (Sigma-Aldrich) diluted in 70 % ethanol for 30 min before washing and mounting. Antibodies used were YAP1 (Cell Signaling; #4912 and #14074), TAZ (Sigma-Aldrich; HPA007415), CK19 (DHSB; TROMA-III), Amylase (Santa Cruz; sc-12821 and Sigma-Aldrich; A8273), GFP (Abcam; ab6673), STAT3 (Cell Signaling; #4904), p-STAT3 (Tyr705; Cell Signaling; #9131), LIFR (Santa Cruz; sc-659) and F4/80 (eBiosciences; #14-4801).

Confocal images were acquired on Zeiss 710, 780 or 880 confocal microscopes and processed using Zeiss AxioVision or Zeiss ZEN software. For quantifications, images

of the whole pancreatic area of three different levels for each mouse were acquired on the Zeiss Axio Scan.Z1 slide scanner, processed and quantified using the Zeiss ZEN software.

TUNEL assay was performed on paraffin-embedded sections using the DeadEnd Colorimetric TUNEL system (Promega) according to manufacturer's protocol.

Immunofluorescence staining in PANC1 cells was performed on glass coverslips. Cells were grown on glass coverslips and fixed for 10 min on ice with 4 % paraformaldehyde. After washing, cells were blocked in blocking solution for 1 h at RT and then incubated overnight at 4 ºC with YAP1 (Cell Signaling; #4912) or TAZ (Sigma-Aldrich; HPA007415) antibodies diluted in blocking solution. Cells were then washed and incubated for 2 h at RT with secondary antibodies (Life Technologies) diluted in blocking solution containing 0.75 nM DAPI. After three washes with PBS, cells were mounted and confocal images were obtained with a Zeiss 710 confocal microscope.

Gene set enrichment analysis

Gene set enrichment analysis was performed on the published transcription profile of C57BL/6 Jackson mice treated with caerulein or PBS [6] and on the transcription profile of mouse liver organoids overexpressing YAP1 [7]. The settings in all analyses were: number of permutations = 1000, permutation type = gene set, enrichment statistics = weighted, metric for ranking genes = t-test. The identified gene sets (nominal p-value $P<.05$) were rank-ordered by normalized enrichment score (NES). Published gene signatures used were: YIMLAMAI_YAP_LIVER [7], CORDENONSI_YAP_CONSERVED_SIGNATURE [8], LABBE_WNT3A_TARGETS_UP [9], YAP_ZHAO_MCF10AND3T3 [10],

REACTOME_SIGNALING_BY_WNT [11, 12], DANG_MYC_TARGETS_UP [13], ALFANO_MYC_TARGETS [14], HAN_JNK_SIGNALING_UP [15], ABBUD_LIF_SIGNALING_1_UP [16], PID_IL6_PATHWAY [17], MTOR_UP.V1_UP [18], HINATA_NFKB_TARGETS_FIBROBLASTS_UP [19], DASU_IL6_SIGNALING_UP [20], AZARE_STAT3_TARGETS [21], PARENT_MTOR_SIGNALING_UP [22], DAUER_STAT3_TARGETS_UP [23], NGUYEN_NOTCH1_TARGETS_UP [24], VILIMAS_NOTCH1_TARGETS_UP [25], TGFB_UP.V1_UP [26] and BIOCARTA_IL6_PATHWAY [27, 28].

shRNA knockdown

Human PANC1 cells stably expressing non-targeting shRNA (shNT) or two independent shRNAs against *YAP1* and *TAZ* (shYAP1/TAZ-#1 and -#2) were generated using lentiviral-based vectors pLL3.7-GFP (Addgene #11795) for shRNA against *YAP1* and tetracycline-inducible pLKO-Tet-On-PURO (Addgene #21915) for shRNA against *TAZ* and selected for GFP signal and puromycin resistance. shRNA sequences were:

shTAZ-#1: 5'-GCCCTTTCTAACCTGGCTGTACTCGAGTACAGCCAGGTTA GAAAGGGCTTTTTG-3';

shTAZ-#2: 5'-CAGCCAAATCTCGTGATGAATCTCGAGATTCATCACGAGA TTTGGCTGTTTTTG-3';

shYAP1-#1: 5'-CCCAGTTAAATGTTCACCAATCTCGAGATTGGTGAACA TTTAACTGGGTTTTTG-3';

shYAP1-#2: 5'-CAGGTGATACTATCAACCAAACTCGAGTTTGGTTGA TAGTATCACCTGTTTTTG-3'.

ACCEPTED MANUSCRIPT

Quantitative RT-PCR

RNA was isolated from dissected pancreata using Qiagen Micro-RNA kit (Qiagen) or from primary acinar cells using the Qiagen Mini-RNA kit (Qiagen) or the MagMAX Total RNA isolation kit (Life Technologies). The cDNA was generated using the Transcriptor First Strand cDNA synthesis kit (Roche Diagnostics) and was used for qPCR SYBR-green (Life Technologies) detection using the primers listed in **Supplementary Table 1**.

Human Pancreatic Tissue Array

Human YAP1 and TAZ protein levels were examined on the human pancreatic tissue arrays BIC14011 and PA207, consisting of pancreatitis, PanIN and PDAC, purchased from US Biomax, Inc. Cores were stained with YAP1 (Cell Signaling; #4912) and TAZ (Sigma-Aldrich; HPA007415) antibodies as described in **Immunofluorescence and immunohistochemistry staining**. The staining intensity was then scored on a scale ranging from 0 (absent) to 6 (strong positive signal).

Chromatin Immunoprecipiation

Chromatin Immunoprecipitation (ChIP) using PANC1 cells with a TEAD4 antibody (Abcam; ab58310) was performed as described [29]. The recovery of DNA was determined by quantitative RT-PCR with SYBR-green (Life Technologies). Primers for quantitative ChIP analysis are listed in **Supplementary Table 2**.

Luciferase expression assay

Luciferase assays were performed in rat acinar AR42J cells with the LightSwitch Luciferase Assay System (Active Motif). The luciferase reporters used were

ACCEPTED MANUSCRIPT

pLightSwitch-STAT3-PROM-722049 (Active Motif) containing 1393 bp of the human *STAT3* promoter (*STAT3* WT), and the same vector where the TEAD binding motif (GT-IIc) 238 bp to 233 bp upstream of the TSS was deleted by site directed mutagenesis (*STAT3* mut GT-IIc). For the positive control, 8xGT-IIc motifs from the YAP/TAZ/TEAD-responsive reporter pGL3b-8xGT-IIc (Addgene #34615) were subcloned into the pLightSwitch empty promoter vector (Active Motif). Cells were co-transfected with pcDNA3 empty vector or the vectors encoding the YAP1 and TAZ phosphorylation mutants pcDNA3-HA-YAP1-5SA and pCS2-FLAG-TAZ-S89A (kind gifts from S. Piccolo). Cells were co-transfected with the pGL3-Control Vector (Promega) to normalize for transfection efficiency.

Supplementary References

1. Takeda K, Kaisho T, Yoshida N, et al. Stat3 activation is responsible for IL-6-dependent T cell proliferation through preventing apoptosis: generation and characterization of T cell-specific Stat3-deficient mice. J Immunol 1998;161:4652-60.

2. Hingorani SR, Petricoin EF, Maitra A, et al. Preinvasive and invasive ductal pancreatic cancer and its early detection in the mouse. Cancer Cell 2003;4:437-50.

ACCEPTED MANUSCRIPT

3. Srinivas S, Watanabe T, Lin CS, et al. Cre reporter strains produced by targeted insertion of EYFP and ECFP into the ROSA26 locus. BMC Dev Biol 2001;1:4.

4. Jackson EL, Willis N, Mercer K, et al. Analysis of lung tumor initiation and progression using conditional expression of oncogenic K-ras. Genes Dev 2001;15:3243-8.

5. Desai BM, Oliver-Krasinski J, De Leon DD, et al. Preexisting pancreatic acinar cells contribute to acinar cell, but not islet beta cell, regeneration. J Clin Invest 2007;117:971-7.

6. Ulmasov B, Oshima K, Rodriguez MG, et al. Differences in the degree of cerulein-induced chronic pancreatitis in C57BL/6 mouse substrains lead to new insights in identification of potential risk factors in the development of chronic pancreatitis. Am J Pathol 2013;183:692-708.

7. **Yimlamai D, Christodoulou C**, Galli GG, et al. Hippo pathway activity influences liver cell fate. Cell 2014;157:1324-38.

8. Cordenonsi M, Zanconato F, Azzolin L, et al. The Hippo transducer TAZ confers cancer stem cell-related traits on breast cancer cells. Cell 2011;147:759-72.

9. Labbe E, Lock L, Letamendia A, et al. Transcriptional cooperation between the transforming growth factor-beta and Wnt pathways in mammary and intestinal tumorigenesis. Cancer Res 2007;67:75-84.

ACCEPTED MANUSCRIPT

ACCEPTED MANUSCRIPT

10. Zhao B, Ye X, Yu J, et al. TEAD mediates YAP-dependent gene induction and growth control. Genes Dev 2008;22:1962-71.

11. Milacic M, Haw R, Rothfels K, et al. Annotating cancer variants and anti-cancer therapeutics in reactome. Cancers (Basel) 2012;4:1180-211.

12. Croft D, Mundo AF, Haw R, et al. The Reactome pathway knowledgebase. Nucleic Acids Res 2014;42:D472-7.

13. Zeller KI, Jegga AG, Aronow BJ, et al. An integrated database of genes responsive to the Myc oncogenic transcription factor: identification of direct genomic targets. Genome Biol 2003;4:R69.

14. **Alfano D, Votta G**, Schulze A, et al. Modulation of cellular migration and survival by c-Myc through the downregulation of urokinase (uPA) and uPA receptor. Mol Cell Biol 2010;30:1838-51.

15. Han SY, Kim SH, Heasley LE. Differential gene regulation by specific gain-of-function JNK1 proteins expressed in Swiss 3T3 fibroblasts. J Biol Chem 2002;277:47167-74.

16. Abbud RA, Kelleher R, Melmed S. Cell-specific pituitary gene expression profiles after treatment with leukemia inhibitory factor reveal novel modulators for proopiomelanocortin expression. Endocrinology 2004;145:867-80.

17. Schaefer CF, Anthony K, Krupa S, et al. PID: the Pathway Interaction Database. Nucleic Acids Res 2009;37:D674-9.

18. Majumder PK, Febbo PG, Bikoff R, et al. mTOR inhibition reverses Akt-dependent prostate intraepithelial neoplasia through regulation of apoptotic and HIF-1-dependent pathways. Nat Med 2004;10:594-601.

19. Hinata K, Gervin AM, Jennifer Zhang Y, et al. Divergent gene regulation and growth effects by NF-kappa B in epithelial and mesenchymal cells of human skin. Oncogene 2003;22:1955-64.

20. Dasu MR, Hawkins HK, Barrow RE, et al. Gene expression profiles from hypertrophic scar fibroblasts before and after IL-6 stimulation. J Pathol 2004;202:476-85.

21. Azare J, Leslie K, Al-Ahmadie H, et al. Constitutively activated Stat3 induces tumorigenesis and enhances cell motility of prostate epithelial cells through integrin beta 6. Mol Cell Biol 2007;27:4444-53.

22. Parent R, Kolippakkam D, Booth G, et al. Mammalian target of rapamycin activation impairs hepatocytic differentiation and targets genes moderating lipid homeostasis and hepatocellular growth. Cancer Res 2007;67:4337-45.

23. Dauer DJ, Ferraro B, Song L, et al. Stat3 regulates genes common to both wound healing and cancer. Oncogene 2005;24:3397-408.

24. Nguyen BC, Lefort K, Mandinova A, et al. Cross-regulation between Notch and p63 in keratinocyte commitment to differentiation. Genes Dev 2006;20:1028-42.

25. **Vilimas T, Mascarenhas J**, Palomero T, et al. Targeting the NF-kappaB signaling pathway in Notch1-induced T-cell leukemia. Nat Med 2007;13:70-7.

ACCEPTED MANUSCRIPT

ACCEPTED MANUSCRIPT

26. Padua D, Zhang XH, Wang Q, et al. TGFbeta primes breast tumors for lung metastasis seeding through angiopoietin-like 4. Cell 2008;133:66-77.

27. **Huang da W, Sherman BT**, Lempicki RA. Systematic and integrative analysis of large gene lists using DAVID bioinformatics resources. Nat Protoc 2009;4:44-57.

28. **Huang da W, Sherman BT**, Lempicki RA. Bioinformatics enrichment tools: paths toward the comprehensive functional analysis of large gene lists. Nucleic Acids Res 2009;37:1-13.

29. Esnault C, Stewart A, Gualdrini F, et al. Rho-actin signaling to the MRTF coactivators dominates the immediate transcriptional response to serum in fibroblasts. Genes Dev 2014;28:943-58.

Author names in bold designate shared co-first authorship.

ACCEPTED MANUSCRIPT